



**TRIBHUVAN UNIVERSITY  
INSTITUTE OF ENGINEERING  
PULCHOWK CAMPUS**

THESIS NO: M-76-MSMDE-2021-2023

**Numerical Study of Wake-Induced Vibration on a Square Prism with Splitter  
Plate, placed downstream of a Larger Circular Cylinder for Piezoelectric Energy  
Harvesting Applications.**

**BY  
ANISH THAPA  
(078MSMDE003)**

A THESIS SUBMITTED TO THE DEPARTMENT OF MECHANICAL AND  
AEROSPACE ENGINEERING IN PARTIAL FULFILLMENT  
OF THE REQUIREMENTS FOR THE DEGREE OF MASTERS OF SCIENCE IN  
MECHANICAL SYSTEM DESIGN AND ENGINEERING

DEPATRMENT OF MECHANICAL AND AEROSPACE ENGINEERING  
LALITPUR, NEPAL

NOVEMBER, 2023

## **COPYRIGHT**

The author has agreed that the library, Department of Mechanical and Aerospace Engineering, Pulchowk Campus, Institute of Engineering may make this thesis freely available for inspection. Moreover, the author has agreed that permission for extensive copying of this thesis for scholarly purpose may be granted by the professor(s) who supervised the work recorded herein or, in their absence, by the Head of the Department wherein the thesis was done. It is understood that the recognition will be given to the author of this thesis and to the Department of Mechanical and Aerospace Engineering, Pulchowk Campus, Institute of Engineering in any use of the material of the thesis. Copying or publication or the other use of this thesis for financial gain without approval of the Department of Mechanical and Aerospace Engineering, Pulchowk Campus, Institute of Engineering and author's written permission is prohibited.

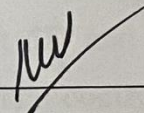
Request for permission to copy or to make any other use of the material in this thesis in whole or in part should be addressed to:

Head  
Department of Mechanical and Aerospace Engineering  
Pulchowk Campus, Institute of Engineering  
Lalitpur, Kathmandu  
Nepal

**TRIBHUVAN UNIVERSITY  
INSTITUTE OF ENGINEERING  
PULCHOWK CAMPUS**

**DEPARTMENT OF MECHANICAL AND AEROSPACE ENGINEERING**

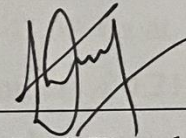
This is to verify that the thesis entitled “Numerical Study of Wake-Induced Vibration on a Square Prism with Splitter Plate, placed downstream of a Larger Circular Cylinder for Piezoelectric Energy Harvesting Applications” submitted by Anish Thapa (078MSMDE003) has been examined and is accepted, in partial fulfillment of the requirements for the degree of Masters in Science in Mechanical Systems Design and Engineering of Tribhuvan University.



Prof. Dr. Mahesh Chandra Luintel

Supervisor

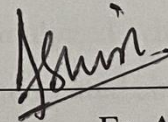
Department of Mechanical and Aerospace Engineering



Asst. Prof. Kamal Darlami

Supervisor

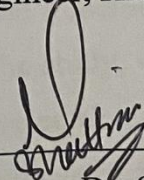
Department of Mechanical and Aerospace Engineering



Er. Ashish Manandhar

External Examiner

MPC Engineer, Himalayan Airlines



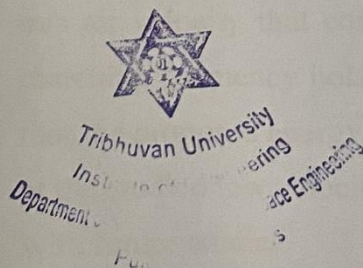
Committee Chairman, Dr. Sudeep Bhattarai

Head

Department of Mechanical and Aerospace Engineering

Pulchowk Campus, Institute of Engineering, TU

Date: 26/11/2023



## ABSTRACT

Flow-induced vibration for energy harvesting is a developing technology, especially at low velocity and small dimensional regimes where conventional turbines are found ineffective. This study numerically explores the wake-induced vibration and interference between galloping and vortex-induced vibration phenomenon on a square prism (12mm) with a splitter plate (60mm length) setup that is placed downstream of another larger circular cylinder (40mm) for piezoelectric energy harvesting applications. Introducing an upstream cylinder created oscillating vortices on the downstream square prism that would otherwise have non-oscillating lift and drag forces. Distance between the bluff bodies was studied at 5D and 3D, D being the diameter of circular cylinder at 4 m/s velocity, and sinusoidal coefficient of lifts with maximum values of 0.85 and 0.98 respectively were obtained. Using splitter plate, the coefficient of lift increased drastically to 2.3 from 0.9. CFD simulation was run from 0.5 m/s to 10 m/s. As the velocity increases, coefficient of lift as well as the vortex shedding frequency increases reaching the maximum of 4.6 and 43.33 Hz at 7 m/s. It was found to follow Strouhal law with an average Strouhal number of 0.213 which agrees with experimental values. But at around 7.5 m/s due to shear layers reattachment between the two bluff bodies, no more oscillating lift is observed, and it is the lock-out velocity for VIV of this harvester. A bistable region can be expected near this velocity region. Beyond it, periodic vortices cease to exist but galloping phenomenon may be observed on further increasing the velocity that can be analyzed with FSI study. FSI Simulation was done for an inlet velocity of 4 m/s which generated sinusoidal emf with peak voltage of 1.2V and 1.59 V for piezoelectric plates of 1mm and 0.3mm thickness respectively. Experiment was carried out on wind tunnel at Pulchowk Campus at 2.18 m/s air velocity that confirmed the sinusoidal pattern of the generated voltage with matching frequency bolstering the numerical study. From the study, we can conclude that the proposed energy harvester has the potential for piezoelectric energy harvesting at the studied low velocity and small dimensional regimes and can be further enhanced with future studies.

**Keywords:** Wake Induced Vibration, Vortex Induced Vibration, Galloping, Fluid Structure Interaction, Piezoelectric Energy Harvesting, Computational Fluid Dynamics, Multi-physics simulation

## **ACKNOWLEDGMENT**

I would like to express my sincere gratitude to Prof. Dr. Mahesh Chandra Luintel and Asst. Prof. Kamal Darlami, for supervising my thesis work with their valuable guidance throughout the work.

I am thankful to the Department of Mechanical and Aerospace Engineering, Pulchowk Campus and Head of Department Dr. Sudip Bhattarai for technical assistance and support by providing access to computational and experimental resources.

I am grateful to all the department professors and lecturers for providing valuable suggestions and kind support throughout the project. I would also like to extend my sincere appreciation to all my classmates for their continuous motivation, support and ideas throughout the project and my family for their constant support and care amid which this thesis work is brought into fruition.

## TABLE OF CONTENTS

ABSTRACT.....	iii
ACKNOWLEDGMENT.....	iv
LIST OF FIGURES .....	vii
LIST OF ABBREVIATIONS.....	x
<b>CHAPTER ONE: INTRODUCTION.....</b>	<b>1</b>
1.1 Background.....	1
1.2 Piezoelectric and Structure Interaction .....	3
1.3 Dimensionless Parameters .....	4
1.3.1 Reynolds Number .....	4
1.3.2 Strouhal Number.....	5
1.3.3 Reduced flow velocity .....	5
1.3.4 Amplitude Ratio.....	6
1.3.5 Aspect Ratio.....	6
1.3.6 Mass Ratio (Added Mass) .....	7
1.3.7 Stiffness Ratio (Added Stiffness) .....	7
1.3.8 Damping Ratio & Added damping .....	8
1.4 Governing Equations .....	9
1.5 Objectives .....	10
1.5.1 Main Objectives:.....	10
1.5.2 Specific Objectives: .....	10
<b>CHAPTER TWO: LITERATURE REVIEW.....</b>	<b>11</b>
2.1 Structural Parameters .....	13
2.2 Piezoelectric Material Properties and Electric Circuitry .....	14
2.3 Fluid Flow Parameters .....	15

2.3.1	SST <i>k-w</i> turbulence model.....	16
2.4	Design Optimization Approaches .....	18
<b>CHAPTER 3: RESEARCH METHODOLOGY .....</b>		<b>21</b>
3.1	Structural Setup.....	22
3.2	Modeling the Fluid-Structure Interaction .....	22
3.3	Validating the Model .....	23
3.4	Optimizing the Model .....	24
<b>CHAPTER 4: NUMERICAL SIMULATION .....</b>		<b>25</b>
4.1	Design Concept.....	25
4.2	Trial Geometries .....	25
4.3	Geometry setup .....	28
4.4	Computational Fluid Dynamics: Fluent solver .....	29
4.5	Turek-Hron Benchmark Test .....	31
4.6	Static and Modal Analysis .....	31
4.7	Transient Structural solver.....	32
4.8	System Coupling: 2-way FSI.....	34
<b>CHAPTER 5: RESULTS AND DISCUSSIONS .....</b>		<b>36</b>
5.1	Static and Modal Analysis .....	36
5.2	Computational Fluid Dynamics .....	38
5.3	FSI Simulation: System Coupling .....	44
5.4	Experimental Study.....	46
<b>CHAPTER 6: CONCLUSION AND FUTURE ENHANCEMENTS .....</b>		<b>49</b>
6.1	Conclusion .....	49
6.2	Future Enhancements.....	49
<b>REFERENCES.....</b>		<b>50</b>

## LIST OF FIGURES

Figure 1: A Bistable Piezoelectric Energy Harvester setup (Qin et al., 2019) .....	3
Figure 2: Physical prototype of a conventional 1DOF piezoelectric harvester (Wang J, 2020) .....	3
Figure 3: Methodology of the research .....	21
Figure 4: Different trial geometries .....	26
Figure 5: Experimental geometry for manipulating natural frequency. ....	27
Figure 6: Structured mesh and dimensions of fluid domain .....	29
Figure 7: Fully developed parabolic velocity profile for Turek-Hron benchmark .....	31
Figure 8: Lift and drag of Turek Hron benchmark a) and b) and the obtained lift and drag c) and d) from simulation respectively at Reynolds no. of 200 .....	33
Figure 9: Fixed support and FSI interface .....	34
Figure 10: Stress due to gravity on the solid structure.....	36
Figure 11: Dimension of the solid structure .....	37
Figure 12: Coefficient of Lift and Velocity contour for cylindrical bluff body of diameter 40 mm for inlet velocity of 4 m/s.....	38
Figure 13: Numerical simulation using double flat plates upstream of circular cylinder showing a) velocity contour at time $t = 5s$ , b) coefficient of lift, and c) coefficient of drag. ....	39
Figure 14: Coefficient of Lift, Drag and Velocity contour for square cylinder without (fig. a, b and c) and with cylindrical bluff body upstream at $L=3D$ (fig. d, e and f) for inlet velocity of 4 m/s. ....	40
Figure 15: Coefficient of lift of square prism with larger circular cylinder upstream for velocity of a) 0.5, b) 1, and c) 2 m/s .....	41



Figure 16: Coefficient of lift of square prism with larger circular cylinder upstream for velocity of a) 4, b) 6, and c) 8 m/s .....	42
Figure 17: Coefficient of lift of square prism with larger circular cylinder upstream for velocity of a) 10, b) 7.8, and c) 7.5 m/s .....	43
Figure 18: Non-vibrating vortex shedding frequency at different velocities.....	44
Figure 19: Values of maximum, average and minimum voltages generated for inlet velocities of a) 1 m/s, b) 4 m/s and c) 10 m/s .....	45
Figure 201: Experimental setup at wind tunnel in Pulchowk campus.....	46
Figure 210: Fabrication process for experimental study.....	46
Figure 22: Flow Visualization at $Re = 1354$ at wind tunnel in Pulchowk Campus.....	47
Figure 23: Experimental value of Positive Voltage readings of PZT sensor through arduino interface .....	48
Figure 24: Average Voltage obtained from FSI Simulation.....	48

## LIST OF TABLES

Table 1: Properties of Structural Member .....	29
Table 2: Properties of Fluid .....	30
Table 3: Calculation for different CFD Cases from inlet velocity 0.5 to 10. ....	30
Table 4: Lift and Drag comparison to Turek -Hron benchmark .....	31
Table 5: Anisotropic Elasticity matrix of Piezoelectric material (PZT-5A) (Mide Technology, 2023) .....	34

## LIST OF ABBREVIATIONS

CAD	Computer-Aided Design
CFD	Computational Fluid Dynamics
DC	Direct Current
DOF	Degrees Of Freedom
FEA	Finite Element Analysis
FEM	Finite Element Method
FFT	Fast Fourier Transform
FSI	Fluid Structure Interaction
LES	Large Eddy Simulation
LPM	Lumped Parameter Model
MEMS	Microelectromechanical Systems
MEMSIC	Micro Electrical Mechanical System Integrated Circuits
PZT	Lead Zirconate Titanate (A Piezoelectric Material)
Re	Reynolds Number
St	Strouhal Number
VIV	Vortex-Induced Vibration
VPP	Peak To Peak Voltage
Ur	Reduced Velocity
DOF	Degree of Freedom
FEI	Fluidelastic Instability
CIV	Cavitation-Induced Vibration
AIV	Acoustic-Induced Vibration

## CHAPTER ONE: INTRODUCTION

### 1.1 Background

Fluid-Structure Interaction (FSI) is a multidisciplinary field that deals with the complex interactions between fluids and solid structures. It involves the study of how fluid flow affects the deformation and behavior of solid structures, and conversely, how the motion and deformation of structures influence the surrounding fluid flow. Study of FSI is vital for better understanding of a wide range of phenomenon such as fluttering of leaves, locomotion of aquatic and aerial animals, musical instruments, flutter of aircraft surfaces, propeller, cardiovascular system, respiratory system, long bridges, high buildings, power transmission lines, heat exchangers, flexible structures in petroleum mining, etc.

In the recent years, focus has been shifted to renewable energy technologies driven mainly due to negative impact of fossil fuels in the environment. Major sources of renewable energy include solar power, biomass, biogas, geothermal power and power generated from fluid flows. Energy generation from fluid flows refer to usage of wind, river, ocean or tidal flows for energy generation. However, conventional water or wind turbines are inefficient at small flow velocities and small dimensional regimes, thus encouraging to seek new technologies involving fluid solid interactions to extract energy from fluid flows efficiently at low velocity and small dimensional regimes.

Many FSI phenomenon like Vortex Induced Vibration (VIV), galloping, flutter and wake induced vibrations have been considered recently for energy harvesting purposes. VIV occurs when there is resonance of the vortex shedded with the natural frequency of the structure. As the fluid flows around the bluff body, such as a sphere, cylinder, prism, etc. at certain flow velocities cylinder, vortices are shed in its wake, creating periodic changes in pressure and flow velocity. These alternating forces can excite the structure's natural modes of vibration, leading to large oscillations transverse to the fluid flow. But this phenomenon is effective only in its lock-in range (region where vortex shedding frequency is close to one of the natural frequencies of the structure), while it is ineffective in other wind speeds.

Galloping occurs when there is positive feedback between the wind-induced force and the structural deformation of the object, resulting in large amplitude vibrations. Compared to VIV, galloping has a higher amplitude and lower frequency. The most famous occurrence of galloping was the collapse of the original Tacoma Narrows Bridge on 7th November 1940 at 68 km/hr. wind. A structure consisting of only a circular cylinder in cross-flow is immune to galloping. For some geometries, instantaneous velocity and force can be in the same direction. At such case, the simplest representation of galloping by 1DOF motion, the criterion for the occurrence of galloping instability, commonly attributed to Den Hartog, is galloping will occur when  $\frac{dF_y}{d\alpha} > 0$ ; where  $\alpha = \tan^{-1}\left(\frac{\dot{y}}{v}\right)$  and  $F_y = -L\cos \alpha - D\sin \alpha$  such that  $\dot{y}$  is the transverse velocity of the body,  $v$  is the velocity of fluid,  $L$  and  $D$ , are the instantaneous lift and drag forces.

Single DOF VIV and galloping based energy harvesting systems considers only the bending of structure in one direction, mainly transverse to the fluid flow and are easier to design. Flutter is a self-excited vibration that typically occurs at high flow velocities. Also, there are other phenomenon such as Fluidelastic Instability (FEI), Acoustic-Induced Vibration (AIV), Flow-Induced Motion (FIM), Turbulence-Induced Vibration (TIV), Cavitation-Induced Vibration (CIV) etc.

For the energy harvesting, a piezoelectric materials attached to the vibrating structure that can produce an electrical charge when subjected to mechanical stress. By adjusting the structural and geometric parameters of the square prism with splitter, it is possible to match its natural frequency with the frequency of the vortices shed behind the primary circular cylinder. With careful design, a galloping response can be achieved just after the lockout from VIV region thus maximizing energy harvesting and increasing velocity bandwidth for energy harvesting at small scale geometry and low air velocity.

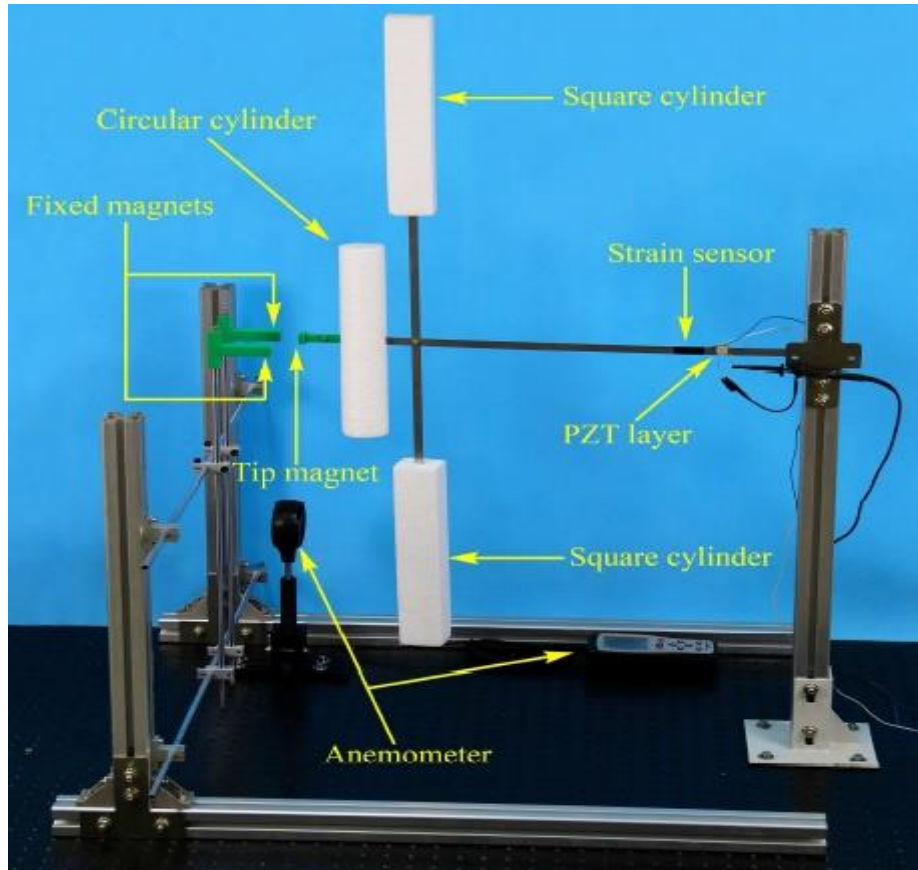


Figure 1: A Bistable Piezoelectric Energy Harvester setup (Qin et al., 2019)

## 1.2 Piezoelectric and Structure Interaction

Certain materials are susceptible to piezoelectric effect and has the ability to produce an electrical charge when subjected to mechanical stress such as vibration, compression, or bending. Piezoelectric materials attached to the vibrating structure can generate electrical energy can be used to power electronic devices or stored for future use.

When the energy generated through the interaction is supplied to external circuit where there is a live load with some resistance, current and some of the generated energy will be consumed there, that will then dampen the vibration. The efficiency of piezoelectric energy harvesting depends on several factors, including

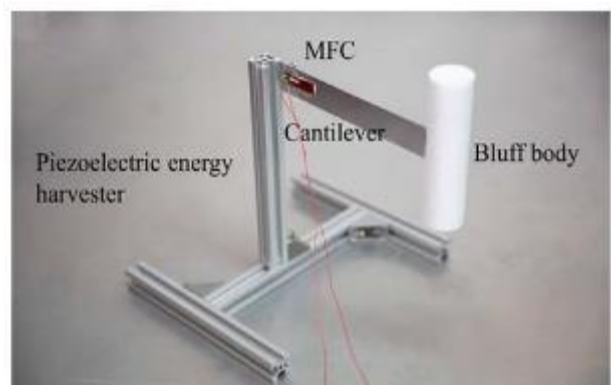


Figure 2: Physical prototype of a conventional 1DOF piezoelectric harvester (Wang J, 2020)

the properties of the piezoelectric material, overall geometry, the electric circuitry and the frequency and amplitude of the mechanical vibrations. These parameters can be optimized in according to our requirement, natural of obtained VIV, physical and geometrical constraints with an aim of modeling more efficient and effective piezoelectric energy harvesters.

### **1.3 Dimensionless Parameters**

In FSI studies, dimensionless numbers are employed to analyze and compare results across different scales and systems, and for model validation and benchmarking. They also help in reducing the complexity of the governing equations, making the analysis more manageable and insightful. Dimensionless numbers also aid in identifying the dominant physical effects within a system. For instance, the Reynolds number signifies whether the flow is laminar or turbulent, while the Strouhal number indicates the vortex shedding frequency. This information is crucial for understanding the behavior of the system and optimizing its design and performance for specific applications. By varying dimensionless numbers, researchers can explore different flow conditions and parameter combinations to maximize the energy generation.

The parameters of this study can be classified into categories such as structural parameters, piezoelectric material properties, electrical parameters and fluid flow parameters. Structural parameters can include mass ratio, stiffness ratio, damping ratio and geometry. Fluid flow parameters can include flow velocity, Reynolds number, Strouhal number and angle of attack. The dimensionless numbers significant for this research are listed as:

#### **1.3.1 Reynolds Number**

Reynolds Number is generally used to dictate whether the fluid flow is steady or turbulent. It is the ratio of inertial forces to viscous forces in a fluid flow. At low  $Re$ , the flow is smooth and laminar, while at high  $Re$ , it becomes turbulent with chaotic motion and vortices. For energy harvesting,  $Re$  is critical as it influences flow behavior and the potential for vortex-induced vibration.

Mathematically, the Reynolds number is:

$$\text{Re} = \frac{\rho * V * L}{\mu} \quad (1.31)$$

where,

$\rho$  is the density of the fluid

$V$  is the characteristic velocity of the flow (e.g., flow velocity past a structure)

$L$  is the characteristic length scale (e.g., diameter of a cylinder)

$\mu$  is the dynamic viscosity of the fluid

The Reynolds number can affect the frequency and amplitude of the VIV, and therefore the energy harvesting performance.

### 1.3.2 Strouhal Number

It is used to identify the critical frequency at which vortex shedding occurs, and it is particularly useful in analyzing the dynamic response of structures subjected to unsteady fluid flows. It is critical number in design vortex-induced vibration energy harvesters, to efficiently calculate lock in and resonance region and velocity. Strouhal number is taken 0.21 for cylindrical bluff bodies for  $300 < \text{Re} < 1.5 \times 10^5$ .

$$\text{St} = \frac{f \cdot L}{V} \quad (1.32)$$

where,

$f$  is the frequency of vortex shedding,

$L$  is the characteristic length scale of the object (e.g., diameter of a cylinder),

$V$  is the fluid flow velocity.

### 1.3.3 Reduced flow velocity

The reduced velocity represents the ratio of the fluid flow velocity to a characteristic velocity of the structure. It signifies the relative strength of fluid forces compared to the inertia of the structure. A large reduced velocity leads to significant dynamic response and fluid-induced vibrations. In contrast, a small reduced velocity results in less pronounced structural vibration. For energy harvesting, an optimal range of reduced velocity enhances power output by efficiently converting fluid flow into mechanical vibrations.



The reduced velocity ( $U_r$ ) is defined as:

$$U_r = \frac{V}{fD} \quad (1.33)$$

where,

$V$  is the fluid flow velocity,

$f$  is the natural frequency of the structure,

$D$  is a characteristic length of the structure (e.g., diameter for a cylinder).

### 1.3.4 Amplitude Ratio

The amplitude ratio refers to the ratio of the maximum amplitude of vibration of a structure (such as a cylinder) to its reference dimension, often its diameter. This dimensionless parameter quantifies the extent to which the structure oscillates in response to fluid-induced forces.

$$AR = \frac{\text{Maximum Amplitude of Vibration}}{\text{Reference Dimension (e.g. Diameter of the Cylinder)}}$$

In the lock-in region, the amplitude ratio can significantly increase. Larger amplitude vibrations can lead to more efficient energy conversion. However, excessive amplitudes can also pose structural integrity challenges, so finding the right balance between vibration amplitude and structural stability is essential in practical applications.

### 1.3.5 Aspect Ratio

The aspect ratio (AR) in this context refers to the ratio of a harvester's characteristic dimension to another relevant dimension. For a prism with splitter plate arrangement, the aspect ratio is usually defined as the ratio of its characteristic length of prism to the length of splitter plate. It can be denoted as:

$$\text{Aspect Ratio} = \frac{\text{Diameter (Characteristics length)}}{\text{Length of splitter plate}}$$

Different aspect ratios can lead to varying flow patterns, resonance behavior, and vibration modes.

### 1.3.6 Mass Ratio (Added Mass)

The mass ratio refers to the ratio of the mass of the vibrating structure to the mass of the fluid displaced due to the motion of the structure. A higher mass ratio results in a lower natural frequency and higher damping, which can reduce the output power.

$$m^* = \frac{m_s}{\rho(\pi D^2/4)} \quad (1.36)$$

where,

$m_s$  is structure mass per unit length,

$D$  is the diameter of the cylinder,

$\rho$  is the density of the fluid.

The added mass ( $m_{\text{added}} = \rho \cdot V_{\text{displaced}}$ ) is a concept used in fluid-structure interaction studies to account for the extra mass that a vibrating structure effectively experiences due to its motion in a fluid medium. It represents the additional mass that the fluid seems to "add" to the moving structure as a result of the fluid's inertia. It can lead to changes in the natural frequencies, amplitudes of vibration, and other mechanical properties of the system.

### 1.3.7 Stiffness Ratio (Added Stiffness)

The stiffness ratio, also termed as the added stiffness quantifies the change in stiffness of a structure due to its interaction with a fluid flow. It is often denoted as  $S_r$  and is calculated as the ratio of added stiffness ( $k_{\text{added}}$ ) to the original stiffness ( $k_{\text{original}}$ ) of the structure.

$$S_r = \frac{k_{\text{added}}}{k_{\text{original}}}$$

The stiffness ratio provides insights into how the fluid-structure interaction influences the overall stiffness characteristics of the system. A higher stiffness ratio implies a more pronounced change in stiffness due to fluid-structure interaction. Studying the stiffness ratio helps to assess the impact on mechanical behavior of the harvester due to fluid forces and can aid in designing systems that are more resilient to FSI-induced effects.

### 1.3.8 Damping Ratio & Added damping

The damping ratio ( $\zeta$ ) in fluid-structure interaction (FSI) refers to the ratio of the actual damping coefficient of a vibrating system to the critical damping coefficient. It quantifies the level of energy dissipation in the system due to damping mechanisms. A higher damping ratio indicates more effective dissipation of energy and faster decay of vibrations.

Added damping, on the other hand, refers to an additional damping term introduced into the equations of motion to account for the energy dissipation caused by the interaction between a structure and the surrounding fluid. This added damping is typically a function of the fluid forces and velocities acting on the structure. It is often introduced to capture the effects of energy loss due to fluid-induced vibrations. It helps in modeling the real-world behavior of structures subjected to fluid flow. The added damping is included in the equation of motion as a way to account for the energy transferred between the fluid and the structure, leading to realistic predictions of the system's dynamic behavior.

The natural frequency of the energy harvester and the frequency of the shredded vortices should resonate to achieve to achieve maximum vibration at the desired synchronization range. By adjusting the geometric parameters and material properties of the energy harvester, it is possible to achieve the desired natural frequency of the energy harvester that is in tune with the frequency of the shredded vortices.

The optimization of these parameters can significantly improve the power output of the harvester. For example, selecting appropriate piezoelectric materials with high coefficients and using compliant mounts can increase power output, while manipulating thickness of the splitter can help us acquire structure with desired natural frequency. Furthermore, optimizing structural parameters, such as stiffness ratio and geometry, can reduce competition between different vibration modes by increase gap between their occurrences.

The parameters in piezoelectric VIV energy harvesters are interdependent. For example, changes in the fluid flow parameters, such as velocity or turbulence intensity, can affect the harvester's structural parameters, such as the natural frequency and damping ratio. Similarly, changes in the structural parameters, such as the stiffness or mass ratio, can

affect the harvester's electrical circuitry and piezoelectric material properties. The following points mentions some of the interdependencies between the parameters.

- The piezoelectric material properties, such as the piezoelectric coefficient and dielectric constant, can affect the electrical output of the harvester. However, change in material also changes the mechanical properties of the material, like its stiffness and damping, which in turn can affect the harvester's resonance frequency and bandwidth.
- The geometry of the harvester, such as its aspect ratio and thickness, can affect the fluid flow parameters around it, such as the vortex shedding frequency and amplitude. This can in turn affect the harvester's vibration amplitude and frequency response.
- The mass and stiffness of the harvester can affect its natural frequency and damping ratio, which can in turn affect its bandwidth and power output.
- The damping ratio can affect the bandwidth and power output of the harvester, but it can also affect the amplitude and frequency response of the harvester, as well as the fluid flow around it.

Overall, these interdependencies make it important to carefully optimize the different parameters of the piezoelectric energy harvester to achieve the best performance. Computational methods can be used to explore the design space and identify the optimal combination of parameters that maximize the performance.

#### 1.4 Governing Equations

The basic governing equations needed for this study are the Navier Stokes equations, structural equations of motion, piezoelectric equation and so on. As the study progress, we may need to further investigate into other equations.

##### Navier Stokes equation

Continuity equation:

$$\nabla \cdot \mathbf{u} = 0 \quad (1.41)$$

Momentum equation

$$\rho \left[ \frac{\partial \mathbf{V}}{\partial t} + (\mathbf{V} \cdot \nabla) \mathbf{V} \right] = -\nabla p + \rho \vec{g} + \mu \nabla^2 \vec{V} \quad (1.42)$$

Equations of motions of vibration

$$m_1\ddot{u}_1 + c_1\dot{u}_1 + k_1u_1 = f_{\text{piezo}} + f_{\text{fluid}} \quad (1.43)$$

$$m_2\ddot{u}_2 + c_2\dot{u}_2 + k_2u_2 = -f_{\text{piezo}} \quad (1.44)$$

Euler–Bernoulli beam theory

$$\frac{d^2}{dx^2} \left( EI \frac{d^2w}{dx^2} \right) = q \quad (1.45)$$

Equation of motion for the free vibrations of the beam:

$$m \frac{\partial^2 w(x, t)}{\partial t^2} + c_s I \frac{\partial^5 w(x, t)}{\partial x^4 \partial t} + c_a \frac{\partial w(x, t)}{\partial t} + YI \frac{\partial^4 w(x, t)}{\partial x^4} = 0 \quad (1.46)$$

Electrical circuit equation for the thin piezoceramic layer attached to the beam:

$$C \frac{\partial v(t)}{\partial t} + \frac{1}{R} v(t) + k \int_0^L \frac{\partial^3 w}{\partial^3 x \partial t} \partial x = 0 \quad (1.46)$$

## 1.5 Objectives

### 1.5.1 Main Objectives:

To examine flow induced vibration on a square prism with splitter plate resulting from wake of a larger circular cylinder placed upstream for energy harvesting applications.

### 1.5.2 Specific Objectives:

- To design the micro scale energy harvester with desired natural frequency such that lock-in (synchronization) occurs at the required velocity range.
- To investigate the two-way system FSI for the wake induced vibration in order to extend the operable range and increase energy output of the piezoelectric energy harvester.
- To study different setup conditions for the bluff bodies in tandem arrangement.
- To iterate the possible parameters to optimize the output energy.

## CHAPTER TWO: LITERATURE REVIEW

Recent years has seen a growing interest in developing energy harvesting systems to extract energy from the environment, such as wind, water, and vibration, to power low-power electronic devices. Among these, piezoelectric energy harvesting has received significant attention due to its simple and efficient design, low cost, and high energy density. There are several ongoing works aimed at extracting energy from cross flow induced vibrations including use of biomimicry, using VIV in pipes, use of flexible materials and use of smart materials.

On Nov 7, 1940, Tacoma Narrows bridge collapsed only four months after its inauguration. It was deducted to be a case of forced resonance, with frequency of vortices being shed matching the bridge's natural structural frequency. It further sparkled researchers' interest to study flow induced vibration. Non-linear resonances, quasi-periodicity, hysteresis phenomena, lock-in, and similar FSI phenomena were extensively studied leading to developments in the field of FSI.

To date, several studies have investigated the use of piezoelectric energy harvesting focusing on optimizing the energy harvesting system's parameters to maximize power output. These parameters can be broadly divided into four major groups namely: structural parameters, piezoelectric material properties, the electrical circuitry and the fluid flow parameters.

The circular cylinder is a classic choice for generating vortex-induced vibration. However, as discussed by Den Hartog (1956), galloping doesn't occur for circular cylinder due to its symmetrical structure. But with a splitter attached behind the cylinder, galloping can be obtained. Rectangular shapes are utilized for galloping energy harvesting. Also, the velocity range for occurrence of galloping is higher than VIV. This study aims to design an energy harvester with enhanced effectiveness and a wider range utilizing both VIV and galloping phenomenon. For this study, a square prism with a splitter plate attached behind it is placed in the wake region of the circular cylinder.

A similar configuration to this study was experimentally investigated by Wang et al. (2021) using wind tunnel tests. A rectangular plate of width  $1D$ ,  $2D$ , and  $3D$  was used and the distance between plate and cylinder was varied from  $0.1D$  to  $2D$ , where  $D$  is

the diameter of a circular cylinder. Their experimental results showed that for a particular plate height, full interference and partial interference between galloping and VIV was observed. After that, lock-in-type response were observed with increasing the space between the plate and the cylinder. The most effective design among the experiment conducted was a 2D-high plate placed around  $0.2D \sim 0.4D$  downstream of the circular cylinder.

Liu et al. (2020), conducted a wide range of experiments with different configurations and provided a promising result with higher voltage output at even low wind speed harvesting utilizing wake induced by using double upstream flat-plates. They found out that placing the double plates upstream of a cylinder can change the vibration response from VIV to galloping, even at a low wind speed. For the square prism the cut-in wind speed decreased from 3.5 m/s to 1 m/s after the double plates are placed upstream, and the output voltage increased significantly from 1 V to 12 V at just 1.5 m/s. The cut-in wind speed can be as low as 1 m/s when the ratios of the horizontal and vertical distances to the windward width of the cylinder were 1 and 0.5, respectively.

Qin et al. (2019), design consisted of a cantilever beam with two square cylinders and a circular cylinder for scavenging wind energy through VIV and galloping. The experiment conducted showed that a large output can be obtained between wind speeds of 2 m/s to 7 m/s. Abdelkefi et al. (2013), used two different upstream cylinders (square in wake of circular cylinder) each attached to vibrating plates and experimented by varying the distances between the cylinders. They concluded that a complex relation exists between cylinders spacing, upstream cylinder size, flow speed, load resistance, and the harvested power output. They designed a galloping based energy harvester with square cylinder that has a cut-in speed of 0.4 m/s and can generate energy at low wind speeds ( $<1.7$  m/s). It was evident that using wake galloping can significantly broaden the speed range on which the harvester can operate. However, the level of enhancement depends on the complex interactions of the wake effects and the spacing distance between the two cylinders.

Apelt et al. from 1973 to 1975, experimented by placing a rigid plate of different length behind a cylinder. They found that drag coefficient and Strouhal number varied when length of the plate to diameter of the cylinder ratio is less than 5 (i.e.  $L/D < 5$ ), due to changes in the near-wake flow patterns. However, if  $L/D > 5$ , then vortex shedding

disappeared and the drag coefficient does not change by changing the length of the plate.

Alam et al. conducted an experimental study using two circular cylinders in a tandem arrangement by varying the spacing between them at a subcritical Reynolds number of  $6.5 \times 10^4$ . Significant changes in parameters like lift, drag, Strouhal number, pressure distribution, and vortex shedding patterns were observed. The well-bistable flow occurred at critical spacing of  $L/D = 3$ , where two values of drag coefficient (CD) were observed as two different flow could exist on that condition; reattachments flow and jump flow. It was evident lift and drag forces on the downstream cylinders are highly dependent to the distance between the cylinders, especially before the critical spacing with two noteworthy peaks at  $L/D = 0.4$  and  $1.40$ . However, for the upstream cylinder, the lift force is undulating, and reached maximum values at  $L/D = 3$  and  $6.25$ , and minimum at  $L/D = 4.5$  and  $8$ . The occurrence of these maximum and minimum values are discussed as due to interaction of the wakes behind the cylinders with ‘in-phase’ and ‘out-of-phase’ conditions, respectively. They also mentioned the work of Sakamoto et al. who noted that coefficient of lift becomes maximum at the critical spacing for the case of two square cylinders due to synchronization of the cylinders with phase lag of  $2\pi$  (in phase).

## **2.1 Structural Parameters**

Structural parameters like stiffness ratio, geometry, mass and damping ratio have a significant impact on the output of piezoelectric energy harvesters. For example, even the use of compliant mounts, which allow for more significant deflection of the piezoelectric material, can increase the power output of the harvester (H. Wei, 2012). Qiu et al. (2017) also confirmed with their work that increasing the diameter of the cylinder and the length of the piezoelectric beam could improve the power output, while increasing the distance between the cylinder and the beam had a negative effect.

In recent years, there has also been increasing interest in using bio-inspired approaches to optimize VIV energy harvesting systems. For example, Zhang et al. (2020) developed a bio-inspired VIV energy harvester based on the shape of fish fins that could significantly enhance the power output compared to a traditional cylinder-based



harvester. Studies have shown that a high stiffness ratio can improve the power output by reducing the competition between the different vibration modes. (Z. Deng 2016). In contrast, a low stiffness ratio can cause the harvester to vibrate in a complex manner, leading to a reduction in power output. (Y. Liu, 2018)

It has been shown that a low mass ratio (i.e., a relatively larger mass of the piezoelectric material compared to the bluff body) can produce an increase in the power output of the harvester. This is because a lower mass ratio results in a higher natural frequency of the system, which can match the frequency of the flow-induced vibrations more closely, resulting in a greater amount of energy being harvested. However, if the mass ratio is too low, it can lead to the piezoelectric material being overloaded and damaged.

Similarly, if the damping ratio is too high, the harvester will dissipate a significant amount of energy and the power output will be reduced. On the other hand, if the damping ratio is too low, the harvester will vibrate longer, which can lead to fatigue failure of the material. It has been shown that increasing the damping ratio can increase the bandwidth of the harvester, which can lead to a higher power output over a wider frequency range. However, this comes at the expense of reduced power output at the resonance frequency of the harvester. (Roundy S. 2004)

## **2.2 Piezoelectric Material Properties and Electric Circuitry**

The piezoelectric material properties also play a critical role in the output of the energy harvester. Zhao et al. (2018) on his computational study found that power output increased with increasing piezoelectric coefficient and decreasing damping ratio, highlighting the importance of selecting appropriate piezoelectric materials for energy harvesting applications. Other important properties include the dielectric constant, quality factor, and electromechanical coupling. Also, the thickness and orientation of the piezoelectric material can play a role.

Electrical circuitry is also important considerations when designing a piezoelectric energy harvester. It should be designed to match the output impedance of the piezoelectric material to the load impedance to maximize power transfer. Research in this area has been focusing on developing more efficient rectifiers and voltage boosters, as well as optimizing the load resistor for specific applications. Additionally, there have been efforts to develop circuitry that can adapt to varying operating conditions, such as

changes in frequency or amplitude of the input vibration. These adaptive circuits can help to maintain a constant power output over a wider range of operating conditions, leading to increased efficiency and operability of the energy harvester.

Huang et al. (2019) proposed a novel approach to increase the power output of a piezoelectric VIV energy harvester by introducing a micro/nano-structure to the surface of the piezoelectric material. They found that this approach enhanced the output voltage and power of the harvester compared to a smooth surface. Another approach is the use of magnetorheological elastomers (MREs) in the energy harvesting system. Wang et al. (2019) developed an MRE-based VIV energy harvester and investigated the effect of parameters like the MRE thickness and magnetic field intensity, on the power output. They found that the power output could be improved by increasing the MRE thickness and magnetic field strength.

### **2.3 Fluid Flow Parameters**

The fluid flow parameters, like the flow velocity, Reynolds number, Strouhal number affects the amplitude and frequency of the vibration. Higher flow velocities can generate larger amplitudes of vibration, which can increase the harvester's power output. However, the turbulence intensity can also cause the harvester to vibrate in a more complex manner, which can lead to a reduction in power output. (Zhang.Y, 2019).

Similarly, Reynolds number which is a ratio of inertial forces to viscous force, can have complex response to the output of the harvester. In general, it has been found that higher Reynolds numbers can produce higher power output of the harvester, due to the presence of stronger and more energetic vortices in the flow. However, there is also a critical Reynolds number above which the harvester's performance begins to decrease due to the onset of flow separation and turbulence. There are studies like done by Yeo and Kim (2012), Xie et al. (2019) which found that the harvester's performance improved with increasing Reynolds number up to a certain point, after which it began to decrease due to flow separation and turbulence.

The Strouhal number is defined as the ratio of the frequency of vortex shedding to the product of the characteristic length of the body and the velocity of the fluid. If the Strouhal number is too low, the harvester may not be able to efficiently capture the

energy from the flow and if the Strouhal number is too high, the flow may become chaotic, leading to a reduction in power output. (Cunha, T. R., 2015).

However, these parameters are interdependent. For example, changes in the fluid flow parameters, such as velocity or turbulence intensity, can affect the harvester's structural parameters, such as the natural frequency and damping ratio. Similarly, changes in the structural parameters, such as the mass ratio or stiffness ratio, can affect the harvester's electrical circuitry and piezoelectric material properties.

### 2.3.1 SST k- $\omega$ turbulence model

The SST k- $\omega$  turbulence model [Menter 1993] is a two-equation eddy-viscosity model that can be used as a Low-Re turbulence model without using extra damping function. The k- $\omega$  formulation is used in internal boundary layer making the model usable upto the wall through the viscous sub-layer. The SST formulation switches to a k- $\epsilon$  behavior in the free-stream making the model not too sensitive for the inlet free-stream turbulences.

#### Transport Equations for the Standard k- $\omega$ Model

(Release 12.0 © ANSYS, Inc. 2009-01-23)

The following transport equations are used for obtaining specific dissipation rate ( $w$ ) and turbulence kinetic energy ( $k$ ):

$$\frac{\partial}{\partial t}(\rho w) + \frac{\partial}{\partial x_i}(\rho w u_i) = \frac{\partial}{\partial x_j} \left( \tau_w \frac{\partial w}{\partial x_j} \right) + G_w - Y_w + S_w \quad (2.31)$$

and

$$\frac{\partial}{\partial t}(\rho k) + \frac{\partial}{\partial x_i}(\rho k u_i) = \frac{\partial}{\partial x_j} \left( \tau_k \frac{\partial k}{\partial x_j} \right) + G_k - Y_k + S_k \quad (2.32)$$

In these equations,  $G_k$  and  $G_w$  are the turbulence kinetic energy generated and generation of  $w$  respectively.  $Y_w$  and  $Y_k$  and represent the dissipation of  $w$  and  $k$  due to turbulence.  $T_w$  and  $T_k$  are the effective diffusivity of  $w$  and  $k$  respectively.  $S_w$  and  $S_k$  are user-defined source terms.

The effective diffusivities for the k- $w$  model are given by

$$\tau_k = \mu + \frac{\mu_t}{\sigma_t} \quad (2.33) \quad \text{and} \quad \tau_w = \mu + \frac{\mu_t}{\sigma_w} \quad (2.34)$$

where  $\sigma_k, \sigma_w$  are the turbulent Prandtl numbers for  $k$  and  $w$ , respectively.

The turbulent viscosity  $\mu_t$  is calculated by as follows:

$$\mu_t = \alpha^* \frac{\rho k}{w} \quad (2.35)$$

### Low-Reynolds-Number Correction

The coefficient  $\alpha^*$  is used to dampen the turbulent viscosity thus enabling a low-Reynolds-number correction which is given by

$$\alpha^* = \alpha^*_{\infty} \frac{(\alpha^*_{\infty} + Re_t/R_k)}{1 + Re_t/R_k} \quad (2.36)$$

The high-Reynolds-number form of the k- $w$  model,

$$\alpha^* = \alpha^*_{\infty} = 1$$

### Production of $k$

The term  $G_k$  is the production of turbulence kinetic energy which is defined as

$$G_k = -\rho \overline{u'_i u'_j} \frac{\partial u_j}{\partial x_i} \quad (2.37)$$

For evaluation of  $G_k$  in accordance to Boussinesq's hypothesis,

$$G_k = \mu_t S^2 \quad (2.38)$$

where  $S$  is the modulus of the mean rate-of-strain tensor.

### Production of $w$

The production of  $w$  is given by

$$G_w = \alpha \frac{w}{k} G_k \quad (2.39)$$

The coefficient  $\alpha$  is given by

$$\alpha = \frac{\alpha_{\infty}}{\alpha^*} \left( \frac{\alpha_0 + Re_t/R_w}{1 + Re_t/R_w} \right) \quad (2.40)$$

where  $R_w = 2.95$ .

The strain rate tensor,  $S_{ij}$  is defined as:

$$S_{ij} = \frac{1}{2} \left( \frac{\partial u_j}{\partial x_i} + \frac{\partial u_i}{\partial x_j} \right) \quad (2.41)$$

Also,

$$\beta = \beta_i \left[ 1 - \frac{\beta_i^*}{\beta_i} \zeta^* F(M_t) \right] \quad (2.42)$$

### Compressibility Correction

The compressibility function, is given by

$$F(M_t) = \begin{cases} 0, & M_t \leq M_{t0} \\ M_t^2 - M_{t0}^2, & M_t > M_{t0} \end{cases} \quad (2.43)$$

where,

$$M_t^2 = \frac{2k}{a^2}, \quad M_{t0} = 0.25, \quad \text{and,} \quad a = \sqrt{\Gamma RT}$$

## 2.4 Design Optimization Approaches

Several studies have used computational methods to optimize the parameters for energy harvesting from cross flow induced vibrations. For instance, Yu et al. (2020) conducted simulations to investigate the effects of the cantilever beam's parameters, including the length, thickness, and piezoelectric material properties. The results showed that the beam's thickness had the most significant effect on the power output, with thinner beams generating higher power outputs. The authors identified the optimal beam length, thickness, and piezoelectric material properties that produced the highest power output and efficiency.

Similarly, Zhao et al. (2018) used a computational model to study the effect of the piezoelectric material properties on the output power. They found that the power output increased with increasing piezoelectric coefficient and decreasing damping ratio, highlighting the importance of selecting appropriate piezoelectric materials. Similarly, Zhang et al. (2019) used a numerical model to investigate the effect of the structural parameters and found that the optimal dimensions varied with the flow velocity and that the power output could be improved by optimizing the structural parameters. Other studies have investigated the effect of different parameters on piezoelectric energy

harvesting from VIV, such as the orientation and placement of the piezoelectric patches (Zhu et al., 2014; Goushcha et al., 2018) and the effect of the electrical load resistance (Hu et al., 2016).

In addition to the aforementioned parameters, fluid flow parameters also play a crucial role. Kim et al. (2017) used experiments and simulations to investigate the effect of the Reynolds number on VIV energy harvesting from a circular cylinder. They found that the optimal reduced velocity for energy harvesting shifted to higher values as the Reynolds number increased. Likewise other fluid parameters such as reduced velocity, fluid density, angle of attack can play a significant role. The synchronization region of an harvester involving a circular bluff body can be expanded through the introduction of various nonlinearities.

Research by Mackowskia and Williamson (2019) has experimentally demonstrated that employing cubic and quintic hardening stiffness, outperform linear models in terms of operable wind speed range. Further enhancements can be achieved through the implementation of bi- or tri-stable stiffness (Smith et al., 2020). Huynh et al. (2021) introduced a nonlinear stiffness that combines the advantages of both bi-stable and hardening stiffness. Magnet-induced nonlinearities have also been explored to enhance restoring forces (Brown & Jones, 2018). The adjustability of magnet-induced force nonlinearity has shown potential to outperform traditional nonlinear springs in broadening the synchronization range of VIV. However, such nonlinear stiffness enhancements often have limitations since they do not alter the aerodynamic properties of the circular cylinder.

An alternative strategy for broadening the effective wind speed range is modifying the aerodynamics of the circular configuration. Slight alterations in the circular structure can lead to significant changes in its flow-induced vibrations (Chen et al., 2017). Aerodynamic modifications, such as those caused by rain rivulets on stay-cables or ice accretion on pipelines (Johnson & Smith, 2019), can induce galloping vibrations, posing structural safety risks. However, these galloping vibrations can be beneficial for aeroelastic energy harvesting, offering a broad effective wind speed range beyond the onset speed of galloping. Research by Bernitsas and colleagues (2020) has demonstrated that the introduction of passive turbulence controls, such as rough strips, to a circular cylinder can enhance vibration responses compared to a smooth surface.

Occasionally, galloping occurs along with or immediately after VIV, a phenomenon known as interfered VIV-galloping (White & Brown, 2018). Hu et al. (2019) experimentally showed that the effective wind speed range of a circular prism based energy harvester can be expanded by installing small-diameter cylindrical rods on its sides.

Similarly, Song et al. (2020) found that attaching a splitter plate behind a circular cylinder trigger galloping vibrations and a  $0.65D$  splitter plate length is found to optimally boost the effective wind speed range for energy harvesting. Wang et al. (2021) investigated the impact of splitter placement on VIV-based energy harvesting, determining optimal angles that greatly enhance performance. Zhu and Gao (2017) suggested symmetrically attaching fin-shaped strips for enhancing energy harvesting of a circular cylinder, achieved successful power harnessing. Moreover, studies by Zhang et al. (2018, 2019) delved into the influence of downstream interference structures on VIV-based energy harvesters, highlighting the benefits of a rectangular plate configuration.

### CHAPTER 3: RESEARCH METHODOLOGY

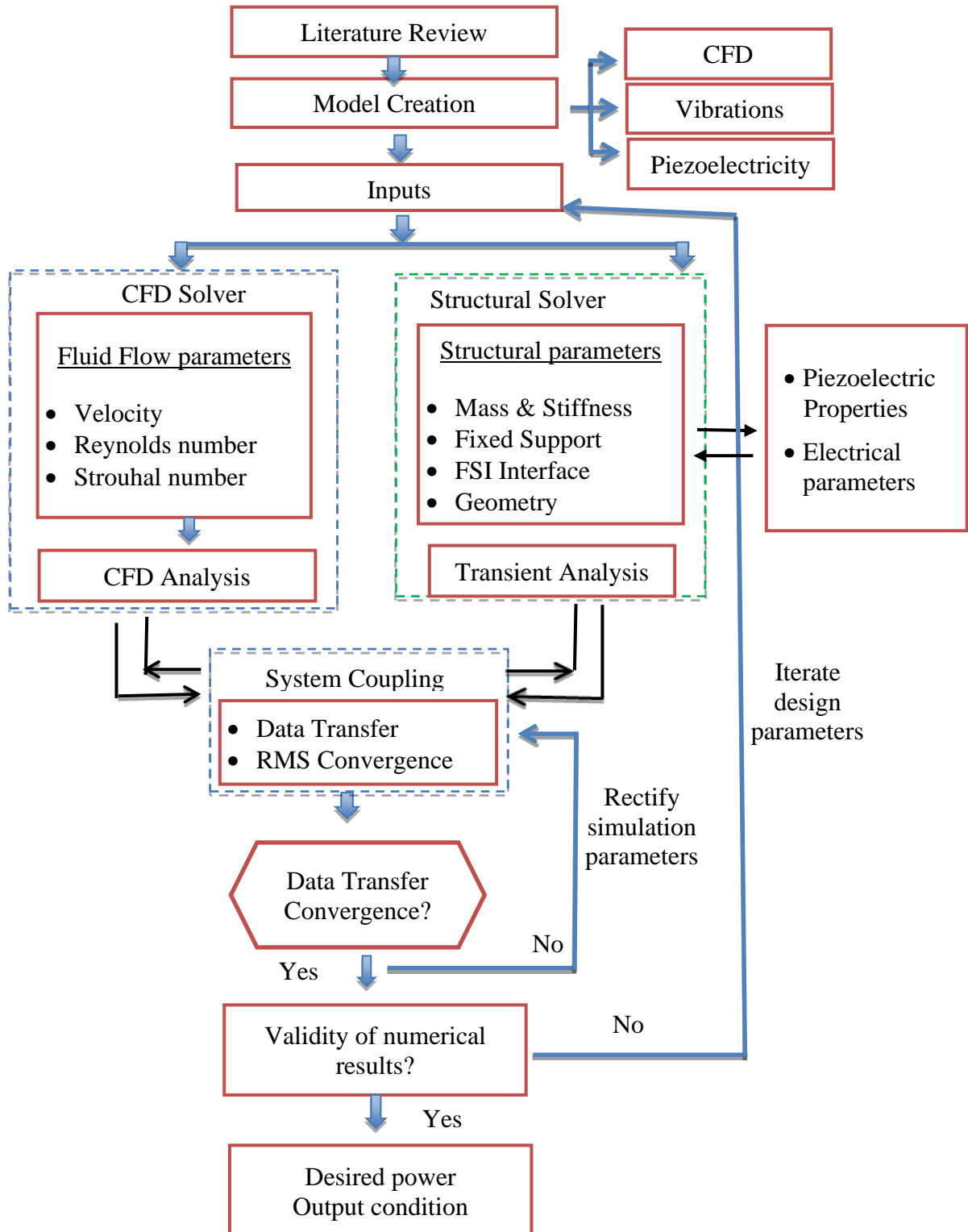


Figure 3: Methodology of the research



### **3.1 Structural Setup**

Geometric properties of the energy harvester include its length, width, thickness, and shape. These properties are important because they affect the harvester's natural frequencies, mode shapes, and overall performance. In addition, the material properties of the harvester, such as its Young's modulus, density, piezoelectric coefficients, and Poisson's ratio, also play a significant role in its performance.

The structural experimental setup typically involves mounting the harvester in a fluid flow, either in a wind tunnel and subjecting it to various flow velocities and conditions. The harvester is typically mounted on a support structure or fixture allowing it to vibrate freely in response to the fluid flow.

The electrical circuitry used to measure and harvest the electrical energy generated by the harvester typically includes a load resistor, an amplifier, and a rectifier. The load resistor is used to simulate the electrical load that the harvester will be powering, and the amplifier is used to amplify the small electrical signal generated by the harvester to a measurable level. The rectifier is used to convert the AC electrical signal generated by the harvester into a DC signal that can be stored in a battery or used to power a device.

The experimental setup should be designed to simulate the conditions under which the harvester will be operating. For example, we should consider the dimensionless numbers such that required flow conditions are achieved. Similarly, if the harvester is designed to operate at a particular frequency range, the experimental setup should be designed to measure the properties over that frequency range.

### **3.2 Modeling the Fluid-Structure Interaction**

Modeling the fluid-structure interaction (FSI) process typically involves solving the Navier-Stokes equations for the fluid flow along the equations of motion for the structure and exchanging the results at a small time step. This can be done using numerical methods such as finite element analysis (FEA), finite volume method (FVM), or boundary element method (BEM), etc.

To simulate the FSI, the fluid domain and the structure domain are discretized into finite elements. The equations for the fluid and structure are solved simultaneously and coupling between the fluid and structure domains is achieved through the application of boundary conditions at the interface between the two domains.

The fluid flow around the harvester can be modeled using either laminar or turbulent flow models, depending on the Reynolds number. The choice of the flow model and solving method have a significant impact on the accuracy of the simulation and the computational cost required for the simulation. In addition to the FSI, the electrical circuitry of the harvester can also be modeled and coupled with the FSI model for more better outputs.

Experimental validation of the FSI model is typically done using physical testing of the harvester in a controlled fluid flow environment. This can involve measuring the vibration and electrical output of the harvester under different flow conditions and comparing the results with the simulation predictions.

### **3.3 Validating the Model**

Validating a model is an essential to ensure that the results obtained from the simulation are accurate and representative of the real-world system. There are several methods for validating a model, such as comparing simulation results with experimental data, standard values or analytical solutions.

The validation process of PZT energy harvester involves comparing the model's predicted power output with experimental measurements. This can be done by subjecting the harvester to different flow conditions and measuring the electrical output, which can then be compared to the simulation results. Additionally, the dynamic response of the harvester, such as the amplitude and frequency of the vibration, can also be measured experimentally and compared with the simulation results.

The validation process requires a comprehensive understanding of the experimental setup and measurement techniques used to collect data. The obtained values like Strouhal number, lift, drags etc. can be compared to standard values at that flow regime. The accuracy of the design model can be improved by incorporating more accurate and precise representation of the experimental conditions.

### **3.4 Optimizing the Model**

Optimizing a model typically involves adjusting the model parameters to improve its accuracy or performance. In the case of piezoelectric energy harvesting utilizing wake interactions, optimizing the model involve adjusting the geometric dimensions, orientation, tandem configurations, material properties, or other parameters to maximize the harvester's power output.

One approach to optimizing the model is to use numerical optimization techniques, such as gradient-based optimization or genetic algorithms, to search for the set of parameters that yield the highest power output. This involves running simulations of the harvester under various operating conditions and evaluating the power output for each set of parameters. However, this technique demands very high computational resources. Simpler numerical study and simulations can be run with proper analysis.

Another approach is to compare the output power from the model with the similar experiments. This can help identify areas where the model needs improvement and guide the selection of optimal parameters. Ultimately, the goal of optimizing the model is to create a reliable and accurate representation of the piezoelectric energy harvester that can be used to guide design decisions and improve the harvester's performance. Along the numerical simulations, experiment and theoretical study, design iterations and tests will be run along the way.

## CHAPTER 4: NUMERICAL SIMULATION

### 4.1 Design Concept

The primary design concept is to closely tune the mechanical natural frequency of the harvester to frequency of shedding vortices generated from wake interaction at the desired air velocity. Another important aspect is the enhanced design of the harvester such that the distance between the cylinders and the ratio of their size produces a suitable wake interaction such that VIV and galloping phenomenon can be utilized for maximizing the amplitude of vibration and obtaining a much wider velocity range at which the energy harvester can operate.

Establishing the fixation points for the transient structure, boundary conditions of the fluid flow should be properly determined. There is also an interplay between the piezoelectric material's mechanical deformation and the generated voltage. In the numerical method, solution convergence in both solvers, the fluid dynamics solver (such as ANSYS Fluent) and the structural dynamics solver (such as ANSYS Mechanical), plays a pivotal role in ensuring accurate and reliable simulation results. In fluid dynamics, convergence refers to reaching a steady-state solution where the governing equations are satisfied within a specified tolerance. Similarly, in structural dynamics, convergence is achieved when the displacements and forces satisfy equilibrium conditions to a desired accuracy. The system coupling allows for exchange of data, such as force and displacements at predefined intervals which should also be converged for a consistent fluid-structure solution.

### 4.2 Trial Geometries

The first task was to design a structural setup for VIV. First to analyze the case of cylinder free to oscillate, a parametric geometry as shown in the figure of order around 10cm was drawn. Several dimensional change iterations were carried out. Several trial geometries were tested.

Tapered sections decrease stiffness and also reduced area of substrate plate. But stiffness can be manipulated by thickness and length so not much significant benefit of tapered geometry. Hollow geometry can help to decrease mass within same surface area

that can help to increase natural frequency ( $w_n = \sqrt{k/m}$ ) and thus requiring higher air velocity for frequency synchronization that is not desirable at the moment. It was found out that tapered geometry works to decrease the stiffness and also reduced the area of the plate on which piezoelectric material is to be mounted.

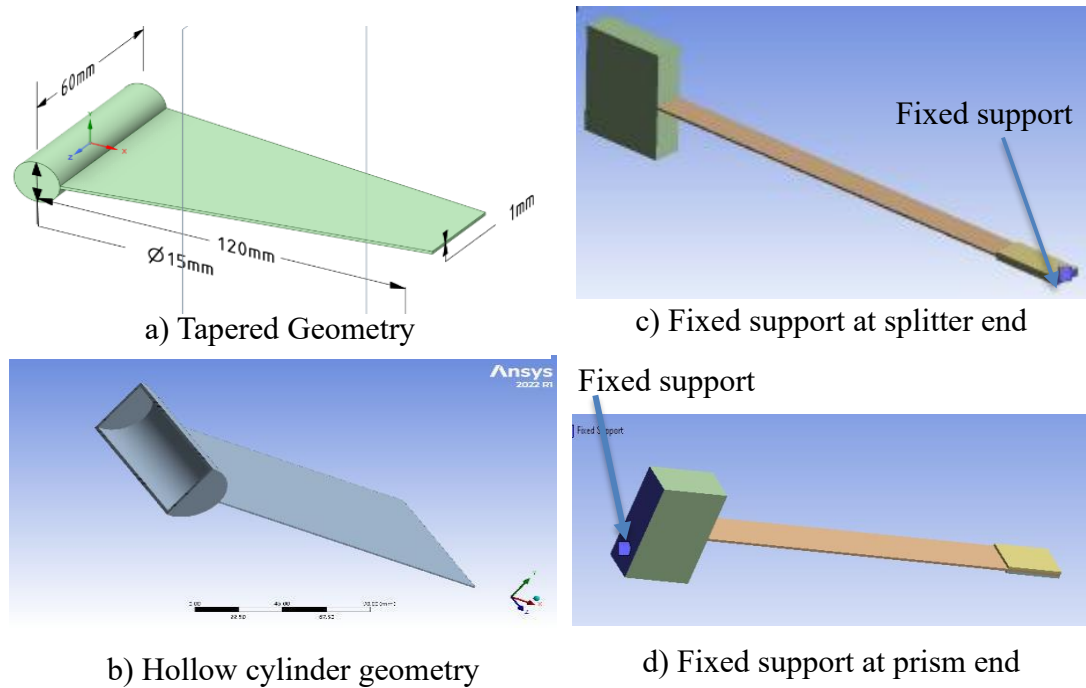


Figure 4: Different trial geometries

Likewise, if fixed support is at the end of the splitter plate and prism is fixed it will have low natural frequency since more mass is hanging. When the prism is fixed, the remaining splitter plate only will have a lower mass and will have high natural frequency which is not desirable to our cause. These geometry modification has significant impact on the natural frequency of the structure. For keeping the low natural frequency as to make the structure small the type c) geometry as in figure 5 was found to be most effective.

Stainless Steel is chosen as the substrate material. The geometry had the cylinder of diameter 15mm and length 60mm, plate length 120mm and plate thickness 1mm. This structure had the natural frequency of 22.17 Hz when the end of the plate was fixed. The second, third and fourth modal frequencies were 120.3 Hz, 251.31 Hz and 692.29 Hz respectively.

The Strouhal number for the cylindrical body is taken as 0.21. Using Strouhal law, velocity range of air flow required for the lock in synchronization of this structure was calculated to be around 1.66 m/s to 3.33 m/s. However, in reality phenomenon like added mass, added stiffness and added damping can change the effective natural frequency of the structure, then changing the lock-in frequency. The maximum deflection at the farthest end of the cylinder can be expected in the range of 15mm which is the diameter of the cylinder.

The geometry was redesigned to carry out numerical analysis at the velocity range of around 5m/s. Geometry iterations will take more time to come up with desired natural frequency. Also, it is not physically possible to change geometry of the harvester. So, a fixed geometry harvester operable in the required range of velocity should be developed. A geometry that is expected to enter lock-in phase at velocity range of 4.2m/s to around 7m/s was proposed. The geometric details are as follows:

Cylinder Diameter: 25mm

Cylinder Length: 90mm

Plate Length: 120mm

AR: 4.8

Plate thickness: 1.8mm

Natural frequency: 33.101 F

2<sup>nd</sup> Modal: 135.73 Hz

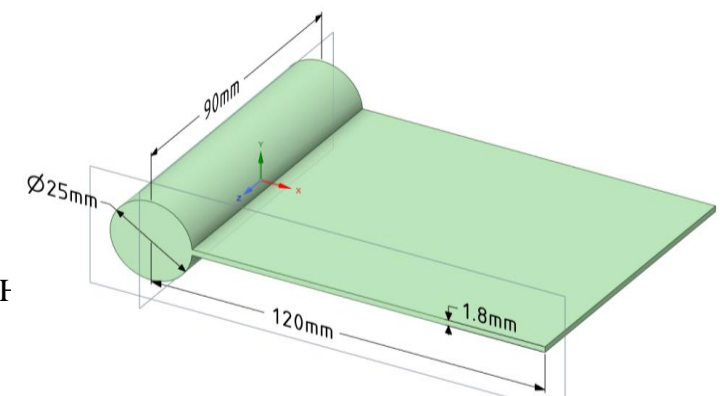


Figure 5: Experimental geometry for manipulating natural frequency.

Air at 20° C

Density: 1.204 kg/m<sup>3</sup>

Dynamic viscosity: 1.825 x 10<sup>-5</sup>

Kinematic viscosity: 1.516 x 10<sup>-5</sup>

During modification of the geometry, it should be noted that:

- i. Increasing diameter decreases natural frequency. But it also decreases shedding frequency
- ii. Increasing length of plate reduces natural frequency.
- iii. Increasing thickness significantly increases natural frequency.
- iv. Increasing length of Cylinder has almost negligible effect on the natural frequency, increases it by almost negligible amount.

Dimensionless analysis with reduced velocity from range 4 to 9 can be an interesting range for study. In case of fixed cylinder, the natural frequency of the structure as shown in figure 5 is 131.44 Hz and the reduced velocity ratio is 1.01 at 4 m/s at which case lock-in doesn't occurs. To increase the reduced velocity either velocity of the flow should be great, which is not controllable in the nature. Or else, the diameter or natural frequency or both should decrease. But the any change in diameter also changes the natural frequency also. Reducing the thickness of the structure decreases stiffness more in proportion than the mass and increases reduced velocity which can be used here.

Increasing the diameter to 40mm, aspect ratio 5 and reducing thickness 1 brings the reduced velocity number closer to 5. More change in this direction will be needed to acquire the proper geometry for lock-in in velocity range of 5m/s. It is evident that the geometry is now around twice the size for free cylinder case. With careful evaluation the reduced velocity in the desired range may be achieved. But there arises another problem that although vortex shedding exists for fixed cylinder in  $300 < Re < 10^6$  range, it goes several transitions of topology and dynamics, and the results are complex and not so well defined. So in this thesis, cases of free cylinder is investigated and fixed cylinder is left for later future studies.

### **4.3 Geometry setup**

For the study of wake induced vibration a square prism with splitter is placed behind relative to the direction of flow in the wake of a larger circular cylinder. In the spaceclaim, a solid geometry was made and a fluid domain was made outside it. From the fluid domain, solid geometry was subtracted. Now, we have a solid geometry and the fluid geometry whose solid geometry part is cut out which can later be given boundary conditions in the fluid solver. A pseudo 3D geometry is made with just a unit thickness in Z direction.

Structured mesh is generated with maximum mesh size less than 5mm. Refinement of order 2 is used in contact area between cylinder and plate. Edge sizing with element size 1mm was done along the length since this is the direction of our interest. Face sizing of 2.5mm was done on the cylinder. Face meshing is done on upper and lower face of plate to obtain structural mesh. The number of nodes and elements was 76,569 and 44,327 respectively.

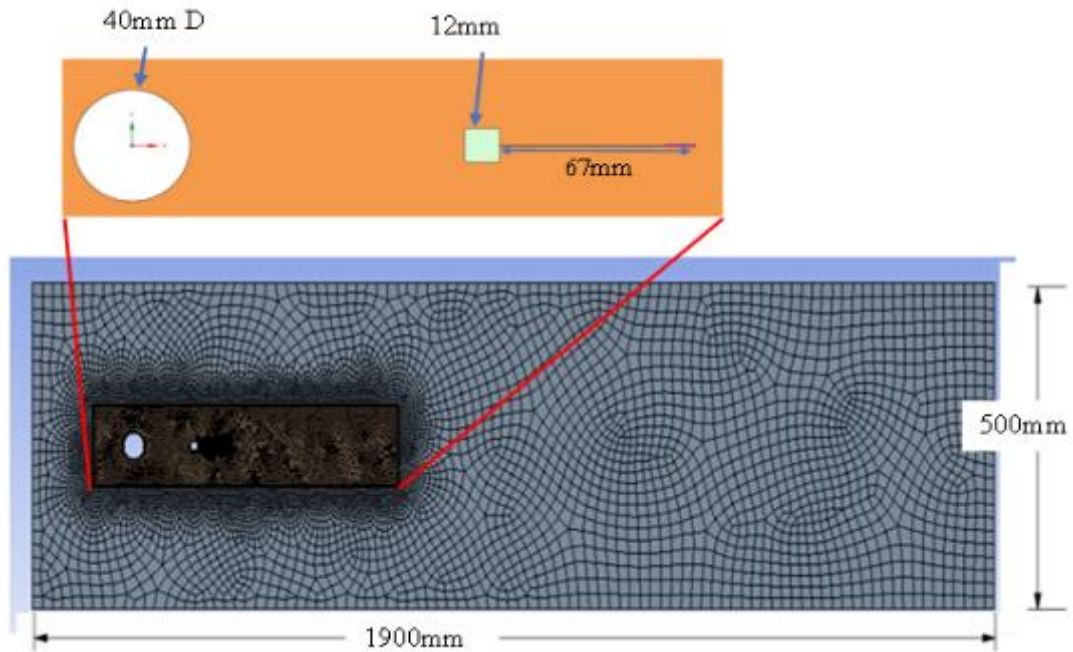


Figure 6: Structured mesh and dimensions of fluid domain

Table 1: Properties of Structural Member

Material	Stainless Steel
Density (kg/m <sup>3</sup> )	7850
Young's Modulus (GPa)	200
Poisson's ratio	0.3

#### 4.4 Computational Fluid Dynamics: Fluent solver

With the motive of engaging both VIV and galloping phenomenon, an upstream circular cylinder of diameter 40 mm and then, a square cylinder of 12mm was placed at distance L between them. The same SpaceClaim geometry file is shared in the fluent solver. Here, the internal solid part is suppressed and the fluid domain has hollow inside it equivalent to the solid. The fluid material is used is air.

Meshing is done with sweep method and body sizing, edge sizing, and inflations to improve mesh quality. Unit cell thickness was kept in Z direction and symmetry boundary conditions were used to further simplify the simulation. Elements order of quadratic is used. Structured mesh is generated with 186,180 nodes and 26,359 elements. Mesh independence condition is achieved. Then the sections of inlet, outlet, fluid wall, fluid body, solid fixed wall and fluid structure geometry were named for further easiness. Pressure based transient solver is selected. In the viscous model SST k-omega model is used.



Table 2: Properties of Fluid

Material	Air
Density (kg/m <sup>3</sup> )	1.225
Dynamic viscosity (kg/ms)	1.789 *10 <sup>-5</sup>

In the boundary condition, inlet velocity magnitude is assigned as per desired reduced velocity number needed. Dynamic meshing options of smoothing and remeshing is used for faces that undergo fluid-solid interaction.

The Turek-Hron benchmark was also successfully run to test the validity of the CFD process. The coefficient of lift and drag as well as animations of pressure and velocity contour was set up to be recorded during the simulation process. Time steps are chosen less than 1/10<sup>th</sup> of the shedding time period. For the energy harvester with natural frequency ( $W_n$ ) = 10.093 Hz (chosen from CFD results) and taking Strouhal number ( $St$ ) = 0.21, the following calculations are done for inlet velocity from 0.5 m/s to 10 m/s.

Table 3: Calculation for different CFD Cases from inlet velocity 0.5 to 10.

Case No.	Inlet velocity, U (m/s)	Reduced Velocity $U_r$	Reynolds No. Re	Shedding Frequency (Hz)	Time period, T (ms)	T/10 (ms)	Simulation time step (ms)
1	0.5	1.24	1,354	2.625	380.95	38.1	20
2	1	2.48	2,707	5.25	190.48	19.05	10
3	2	4.95	5,414	10.5	95.238	9.524	8
4	4	9.91	10,829	21	47.619	4.762	4
5	6	14.86	16,243	31.5	31.75	3.17	3
6	7	17.34	18,950	36.75	27.21	2.72	2
7	7.5	18.58	20,304	39.375	25.40	2.54	2
8	8	19.82	21,657	42	23.81	2.381	2
9	10	24.77	27,072	52.5	19.048	1.905	1

Under the dynamic mesh, system coupling is selected for the five faces that undergoes fluid structure interaction. For the fluid wall and solid fix wall, stationary condition were selected. Coupled scheme is selected in solution method. In the report definition lift and drag reports are added. The residual values in the monitor are set to 0.001. Maximum iterations per time step is set to 100. Hybrid initialization is done with number of iterations 50 and scalar value ending to 6.53e-13. Animation of pressure contour, velocity contour and mesh are recorded for every 5 time step.

#### 4.5 Turek-Hron Benchmark Test

The Turek-Hron benchmark is a widely recognized CFD benchmark used to assess the accuracy and performance of numerical methods in simulating fluid-structure interaction (FSI) problems. It specifically focuses on the VIV of a circular cylinder. The benchmark provides a well-defined scenario where a

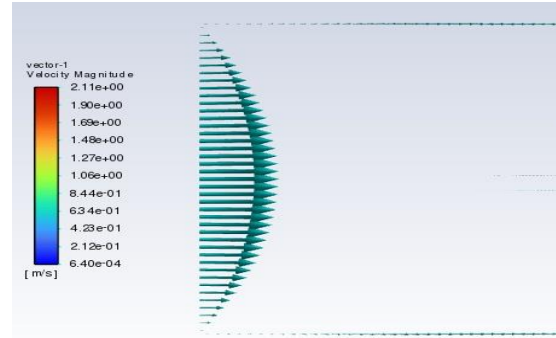


Figure 7: Fully developed parabolic velocity profile for Turek-Hron benchmark

cylinder experiences oscillatory motion due to the interaction with the fluid flow. It is often used to evaluate the accuracy of their simulations, assess the performance of different numerical methods, and validate the results of their models against experimental data. Its standardized nature allows for consistent comparisons between various numerical solvers and helps identify strengths and limitations in different FSI simulation approaches.

Table 4: Lift and Drag comparison to Turek -Hron benchmark

S.No.	Re	Avg. velocity	Quantity	Obtained Value	Standard Value	% Difference
1	20	0.2	Lift	1.1093	1.119	0.87
			Drag	14.18	14.29	0.76
2	100	1	Lift	10.84	10.53	2.9
			Drag	138.29	136.7	1.16

#### 4.6 Static and Modal Analysis

The splitter plate end downstream of the square prism is fixed. Two piezoelectric patches are attached above and below, near the end. The top and bottom faces of the PZT patches were read for voltage output and other sides were given boundary conditions as ground (0 V). The end of the splitter was fixed. Calculations for stress and deformation due to gravity due to gravity is done in Static Structure solver and natural modes of vibrations are computed in the Modal solver which is also shown in the results section. As, VIV phenomenon is the case of resonance and since these pre-stress value doesn't affect the natural frequency of the structure, these conditions can be ignored and need not be pre-initialized for transient analysis. Also, the deformation and loading are due to gravity which is along Y- direction in this geometry and that will

change if we change the orientation of the structure.

The natural frequency of the design geometry is 10.495. This is in close to the calculated shedding frequency of 10.5 Hz at 2 m/s air speed. So, VIV lock in can be expected at this velocity region. The structure can be expected to be in resonance with the shedding frequency when the reduced velocity is around 5 for Strouhal number 0.2, i.e.  $St.Ur=1$ . It is the region where the shedding frequency is close to the natural frequency. At this velocity range there is not possibility of lock-in with other modes of vibration. But if the velocity is increased to as high as 23.687 m/s, second modal vibration of 124.36 Hz can be in resonance which is torsional in nature.

#### **4.7 Transient Structural solver**

The Transient Structural solver in ANSYS employs the Finite Element Method (FEM) to solve dynamic structural problems over time. This solver is used to obtain transient values of parameters of our concerns such as displacement, stress, strain, dynamic force etc. under our given boundary conditions and loading conditions. Unlike static analysis, transient analysis considers inertia and damping effects.

The geometry is imported in transient solver. Outer fluid domain is suppressed. Pre-stress can be defined in initial condition or through use of multiple time steps with time integration setting on or off. But such setup doesn't allow for setting up of Fluid Structure Interaction load. As we have discussed before they are not necessary for this study, we can use fluid structure interaction load and fixed support in the transient solver at the required faces.

Piezoelectric and MEMS extension is added in ANSYS for piezoelectric material. Properties of piezoelectric material PZT-5A was also defined with density of 7750 and anisotropic elasticity matrix as follows. The material properties of the piezoelectric substrate like piezoelectric coefficients, dielectric constants, and mechanical coupling coefficients, all of which significantly dictate the conversion efficiency of mechanical strain energy into electrical voltage.

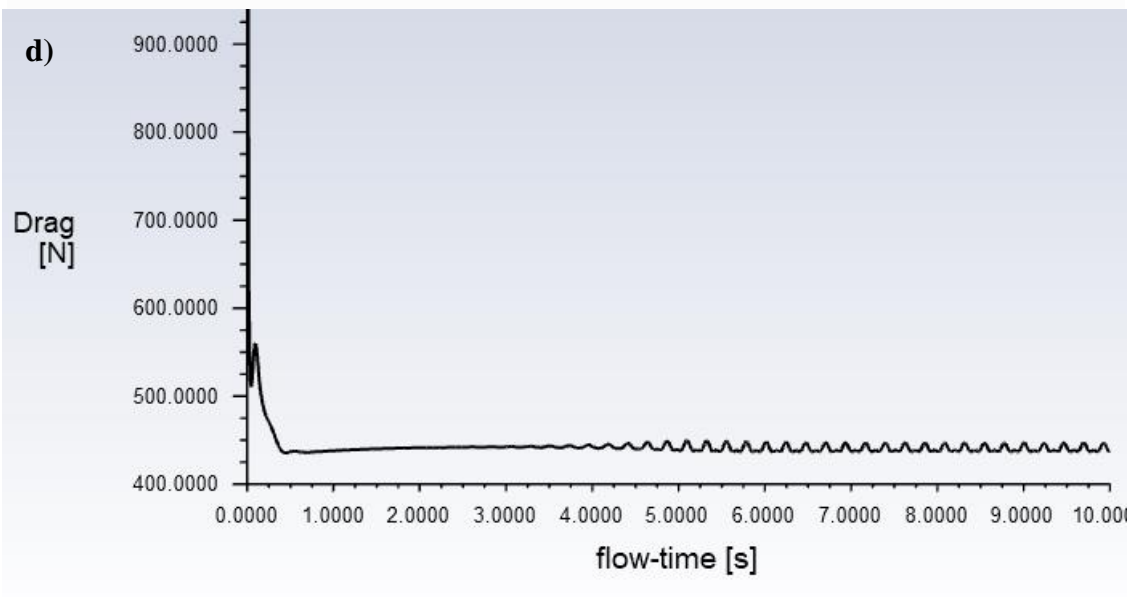
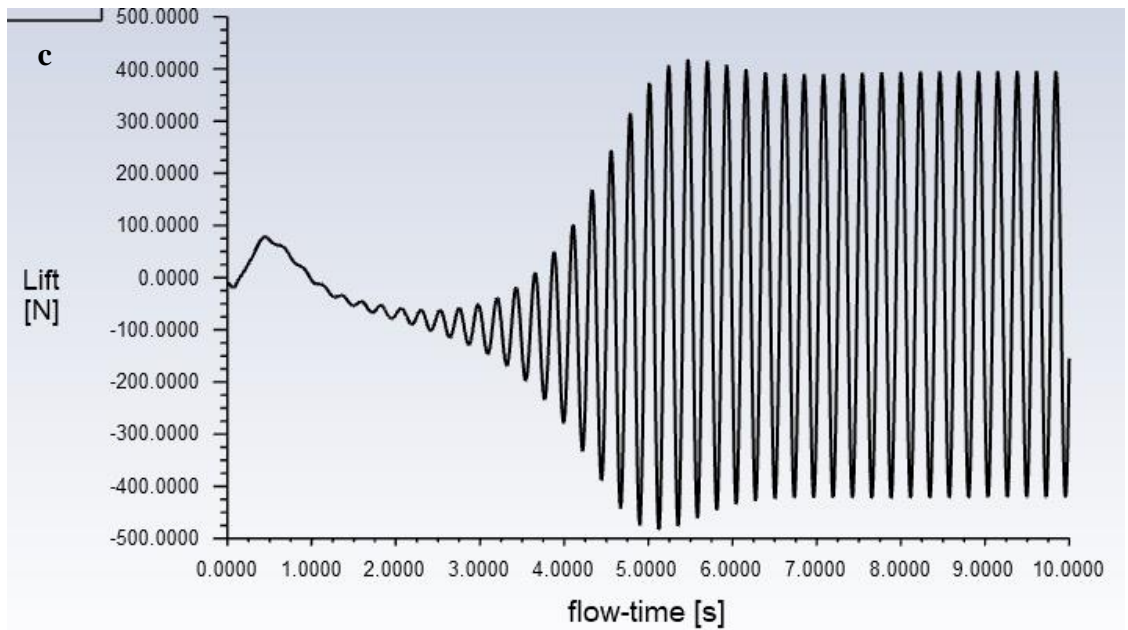
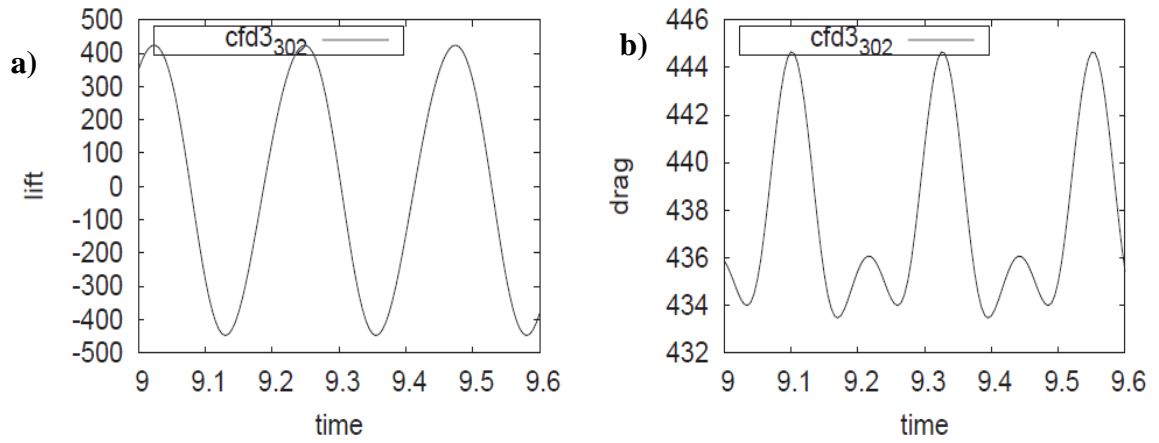


Figure 8: Lift and drag of Turek Hron benchmark a) and b) and the obtained lift and drag c) and d) from simulation respectively at Reynolds no. of 200

The transient structural uses fundamental equation of motion which is:

$$\{F(t)\} = [M]\{\ddot{u}\} + [C]\{\dot{u}\} + [K]\{u\}$$

where,

$[M]$  = mass matrix

$[C]$  = damping matrix

$[K]$  = stiffness matrix

$\{\ddot{u}\}$  = nodal acceleration vector

$\{\dot{u}\}$  = nodal velocity vector

$\{u\}$  = nodal displacement vector

$\{F(t)\}$  = load vector

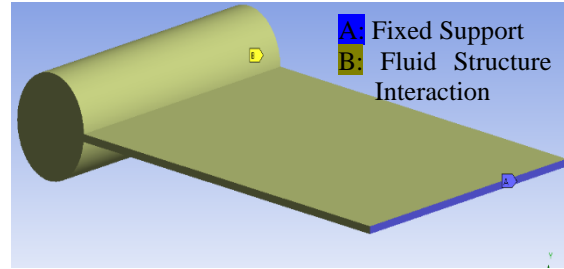


Figure 9: Fixed support and FSI interface

Table 5: Anisotropic Elasticity matrix of Piezoelectric material (PZT-5A) (Mide Technology, 2023)

1.2E+11					
7.51E+10	1.11E+11				
7.52E+10	7.51E+10	1.2E+11			
0	0	0	2.11E+10		
0	0	0	0	2.11E+10	
0	0	0	0	0	2.26E+10

The time step size of the transient solver will be overridden by system coupling setting. But total time of simulation (Step End Time) must be defined. Large deflection should be turned on. Restart points must be enabled to enable the resume of simulation in the PC since each case takes around a week to simulate.

#### 4.8 System Coupling: 2-way FSI

System Coupling is used in ANSYS to solve this Multiphysics problems by connecting independent fluent and transient structure solvers such that bidirectional exchange of solution data may occur at a small timestep in range of a microsecond (equal to time step required within fluent solver) enabling accurate capture of complex fluid structure interaction. Force is transferred from fluent to transient structural solver and displacement from structural solver to fluent. Iterations are carried out until convergence within the solvers and at data transfer is reached to the required values. This exchange enables accurate representation of the dynamic interaction between the fluid and structure, taking into account the forces and displacements generated in both domains.

The end time step of system coupling should be less than or equal to end time of transient structure. Maximum iteration per time step is set to 50. The step size is in range of single digit of microseconds depending on the case. It should be around ten times smaller than the shedding frequency as to not miss the phenomenon.

The first data transfer is created where the force is transferred from fluent structure to transient structure. In the second data transfer incremental displacement is transferred from transient structure to fluent solver. The RMS convergence target for these data transfer is 0.01. Immediate restart data output is set at interval of 5 steps from where we can continue the simulation in case of unexpected shut-downs. After the setup is complete on pressing Update, the system coupling simulation will run involving transient structure and fluent solvers.

Once the simulation is executed, we can observe it in real time in Solution Information panel. One of the first things to ensure is that the fluid structure interaction are properly matched between the solvers. Area mapping should here be 100%.

The convergence should be at the four steps as follows:

- a) Convergence within fluid solver
- b) Convergence within structure solver
- c) Convergence of force transfer from fluid solver to structure solver
- d) Convergence of displacement transfer from structure solver to fluid solver.

Each time step may converge at different number of iterations. It is found that Transient Structure converges early, then first data transfer converges which is force transfer from fluent to transient structure. The next two may take some more iterations to converge, generally incremental displacement from transient structure to fluent being the last to converge.

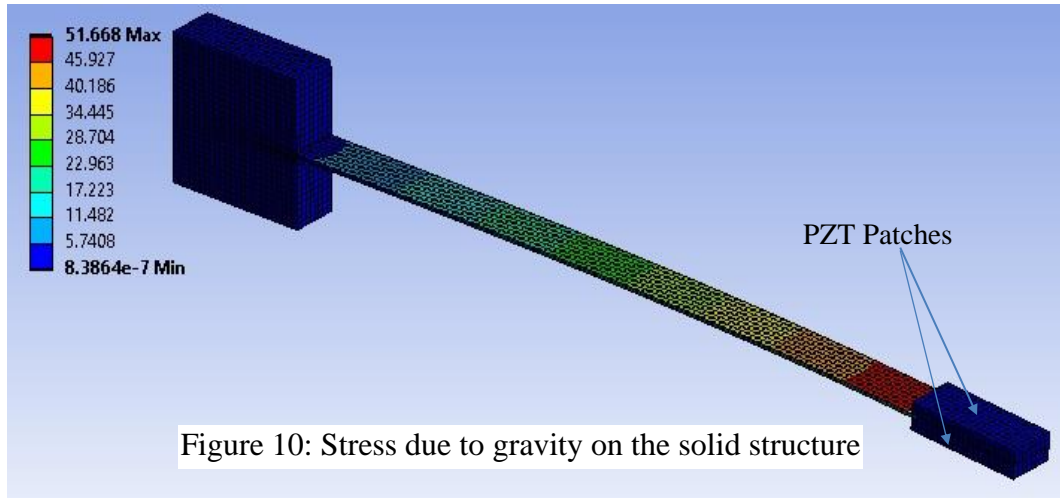
## CHAPTER 5: RESULTS AND DISCUSSIONS

### 5.1 Static and Modal Analysis

The static and modal analysis was done before the transient analysis. The maximum deformation due to its own weight was 2.598 mm at the extreme end and 1.396 mm was the average. The minimum, maximum and average of equivalent stress are 0.72464 Pa, 48.9 MPa and 5.38 MPa respectively. The minimum, maximum and average of equivalent elastic strain are  $1.096 \times 10^{-11}$ ,  $4.4364 \times 10^{-4}$ , and  $3.857 \times 10^{-5}$  respectively. As, VIV phenomenon is the case of resonance and since these pre-stress value doesn't affect the natural frequency of the designed structure, these conditions can be ignored and need not be pre-initialized for transient analysis. Also, the deformation and loading are due to gravity which is along Y- direction in this geometry and that will change if we change the orientation of the structure.

The design of the vibrating structure can be done such that the lock-in can be achieved in the desired velocity range. For this, the harvester's natural frequency should be comparable to the shedding frequency of the vortices. We know that,

$$\text{Shedding Frequency} = (St. v)/D$$
$$\text{Required natural frequency at velocity } v, W_n = v/(Ur.D)$$



During the modal analysis, it was found that piezoelectric patch attached to the structural body, if not fixed or constrained to any relative motion would not significantly affect the natural frequency of the structure. In agreement with the solid mechanics, the following method can be employed to obtain the desired natural frequency of the structure as per our requirement.

It was found that:

- i. Increasing diameter of upstream cylinder also decreases shedding frequency.
- ii. Increasing size of downstream square cylinder ( $D$ ) decreases natural frequency.
- iii. Increasing length of splitter plate ( $L$  and  $AR$ ) reduces natural frequency.
- iv. Increasing thickness of splitter plate ( $t$ ) significantly increases natural frequency.
- v. Increasing length of Cylinder ( $L1$ ) has almost negligible effect on the natural frequency, increases it by almost negligible amount.

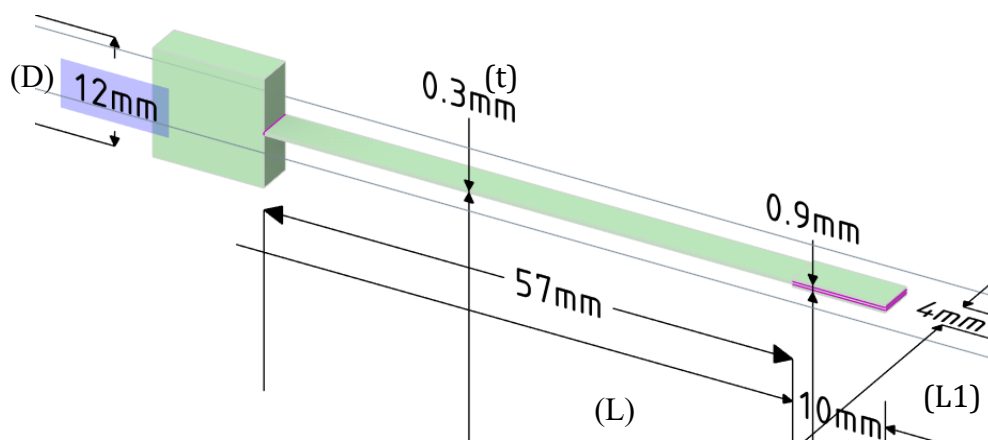


Figure 11: Dimension of the solid structure

With these manipulations, we can create the structure with the desired natural frequency. However, phenomena like added mass, added stiffness, and added damping can slightly change the effective natural frequency and then the lock-in frequency. The structure was designed with the first natural mode of vibration of 10.495 Hz followed by second torsional mode of 124.36 Hz that can match the shedding frequency at 23.69 m/s. The natural frequency of the structure is designed to be 10.495 Hz so that it can be in resonance to the calculated shedding frequency of 10.5 Hz at 2 m/s air speed due to upward circular cylinder. So VIV lock in can be expected at this velocity region as the reduced velocity is around 5 for Strouhal number 0.21, i.e.  $St.Ur=1$ . It is the region where the shedding frequency matches the natural frequency. At this velocity range there is not possibility of lock-in with other modes of vibration.



## 5.2 Computational Fluid Dynamics

At first CFD was done on circular prism with splitter plate attached behind as in figure 9 with diameter of 25mm. The shedding frequency is inversely proportional to the characteristic length. A larger cylinder will have less frequency and 40mm cylinder was also studied for vortex induced vibration. Recent studies have shown that wake induced vibration helps to decrease the lower cut-off velocity and helps increase the velocity range for energy harvesting. So, a square prism with splitter plate behind is used in the wake of larger cylindrical prism.

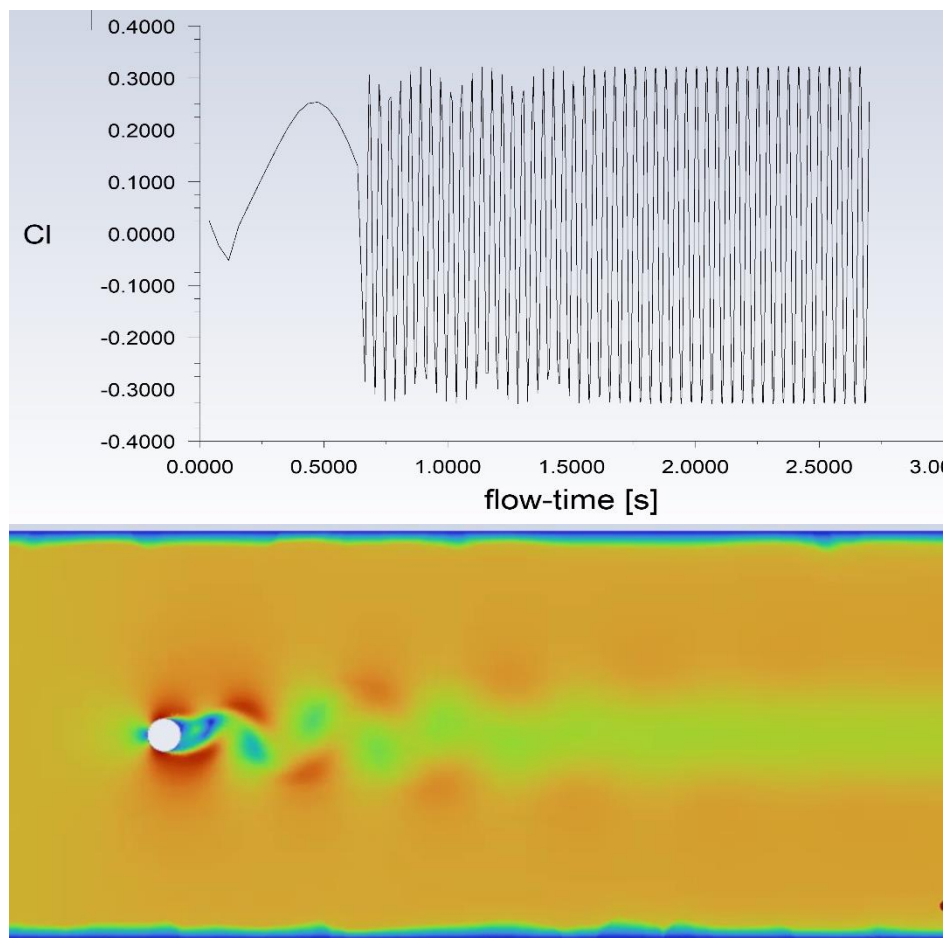


Figure 12: Coefficient of Lift and Velocity contour for cylindrical bluff body of diameter 40 mm for inlet velocity of 4 m/s.

It was observed that using the circular bluff body upstream provided oscillating vortices as in figure 13 on the square prism that would otherwise have non-oscillating small lift and drag forces only, thus enabling the possibility of piezoelectric energy harvesting. Two trials were carried out, keeping the bluff bodies at 5D and 3D distances that produced numerical results for oscillating coefficient of lifts with maximum values of 0.85 and 0.98 respectively.

Another interesting approach was taken by Liu et al. (2020), of using double upstream flat-plates. I tried the method and it looked promising. Lift generated pattern was rather complicated and almost harmonic. But wake induced vibrations of tandem arrangement with circular and square prism provided a better result for now. So, in this research I will stick to the arrangement as in figure 4 c).

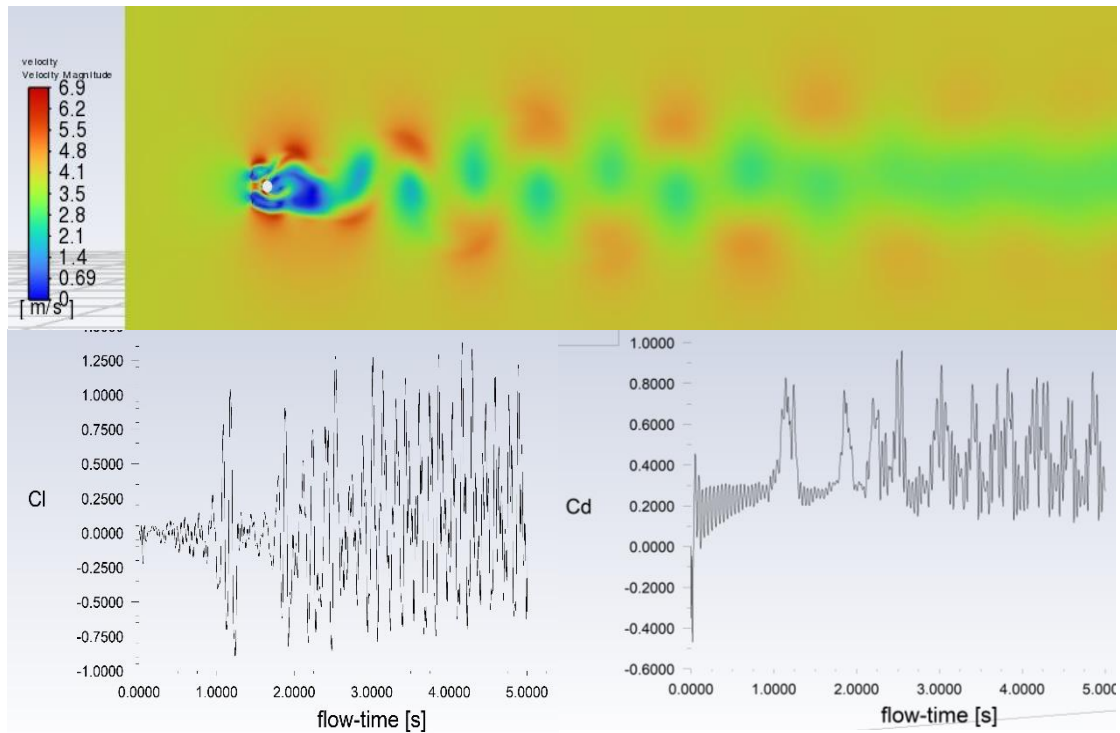


Figure 13: Numerical simulation using double flat plates upstream of circular cylinder showing a) velocity contour at time  $t = 5s$ , b) coefficient of lift, and c) coefficient of drag.

In the circular bluff body upstream of square prism arrangement, a splitter plate was attached behind the square cylinder. The lift coefficient for the square cylinder only increased drastically from 0.98 to 2.3. CFD analysis was done on this setup for velocity ranging from 0.5 m/s to 10 m/s. As the velocity increases lift as well as the vortex shedding frequency increases. But at around 7.5 m/s due to shear layers reattachment between the two bluff bodies, no more oscillating lift is observed. A bistable region can be expected near this velocity range. It is the lock-out velocity region for vortex-induced vibration. Beyond it, periodic vortices cease to exist but galloping phenomenon may be observed that cannot be visualized by only CFD but requires multi-physics simulation between the fluid and solid domain i.e., FSI. The lift generated on various velocities between 0.5 m/s to 10 m/s are shown in figure 15, 16 and 17.

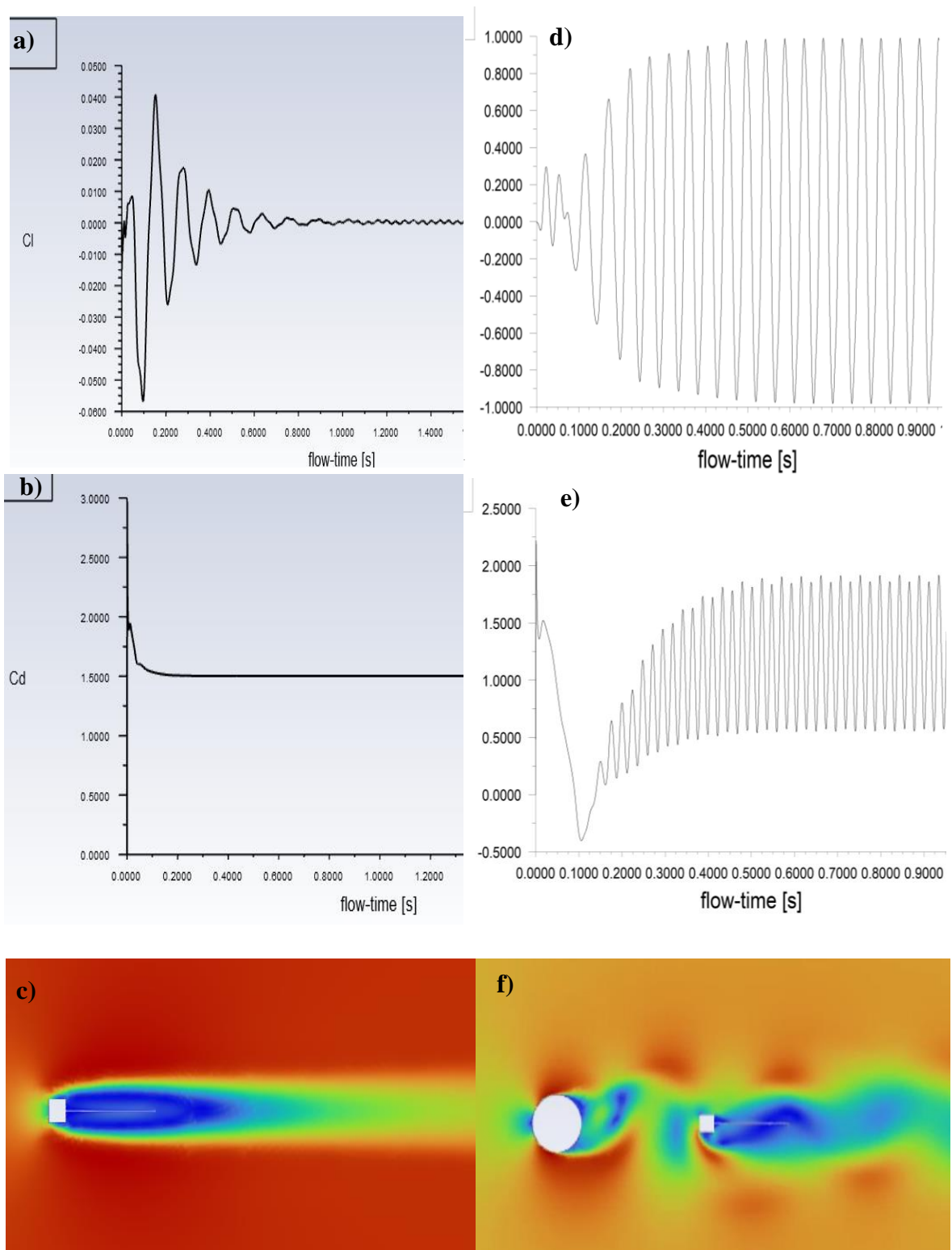


Figure 14: Coefficient of Lift, Drag and Velocity contour for square cylinder without (fig. a, b and c) and with cylindrical bluff body upstream at  $L=3D$  (fig. d, e and f) for inlet velocity of 4

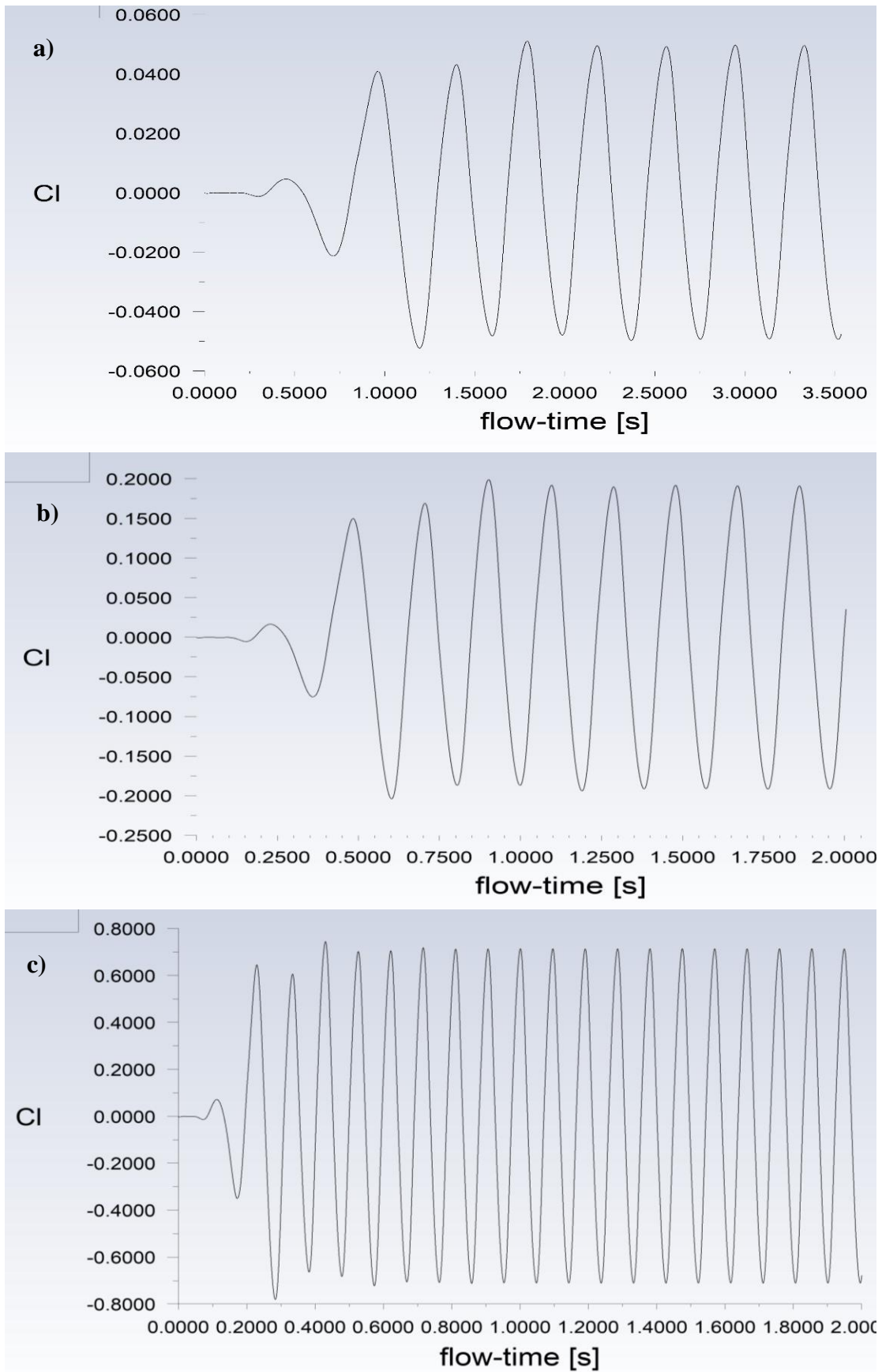


Figure 15: Coefficient of lift of square prism with larger circular cylinder upstream for velocity of a) 0.5, b) 1, and c) 2 m/s

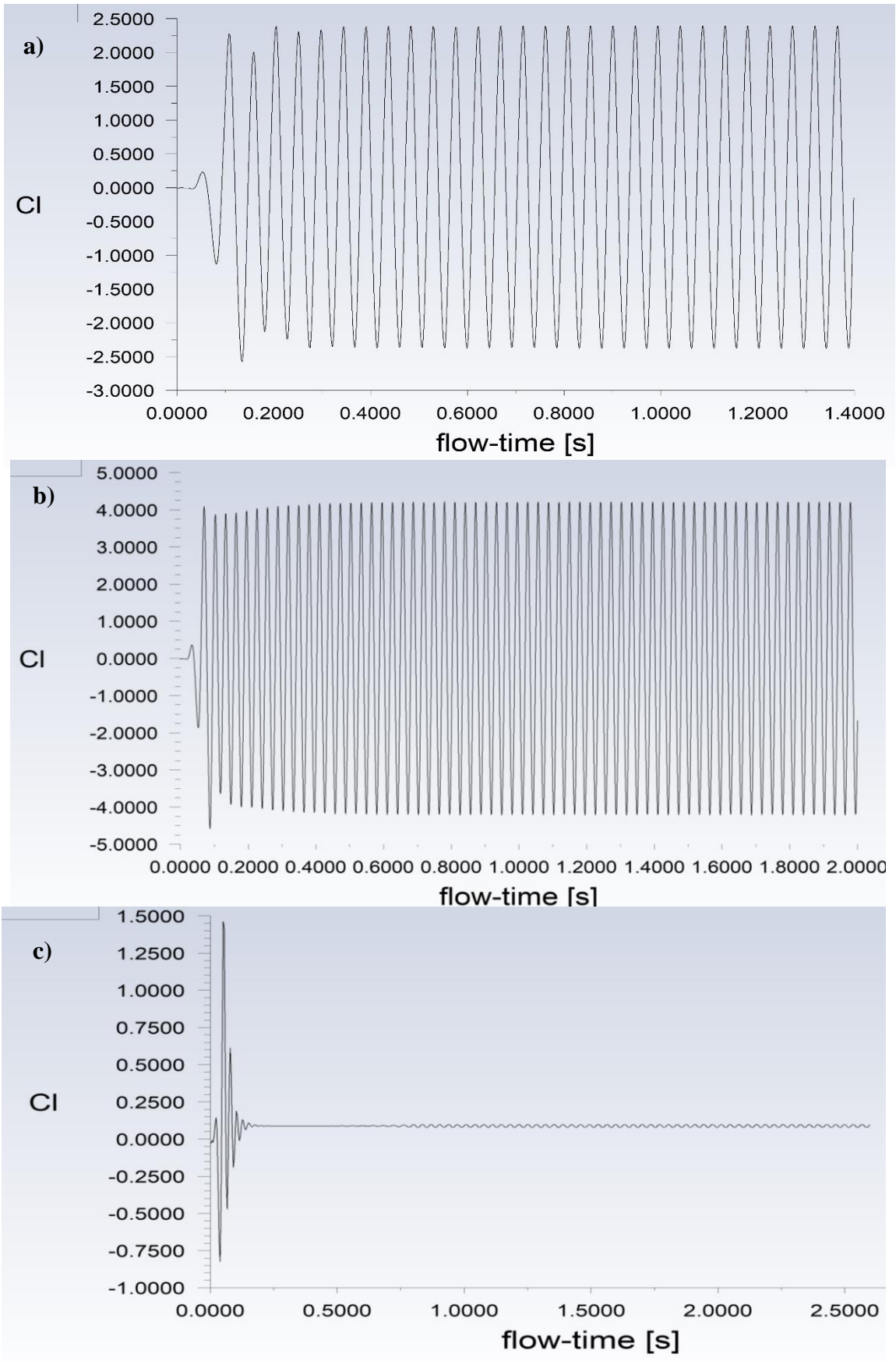


Figure 16: Coefficient of lift of square prism with larger circular cylinder upstream for velocity of a) 4, b) 6, and c) 8 m/s

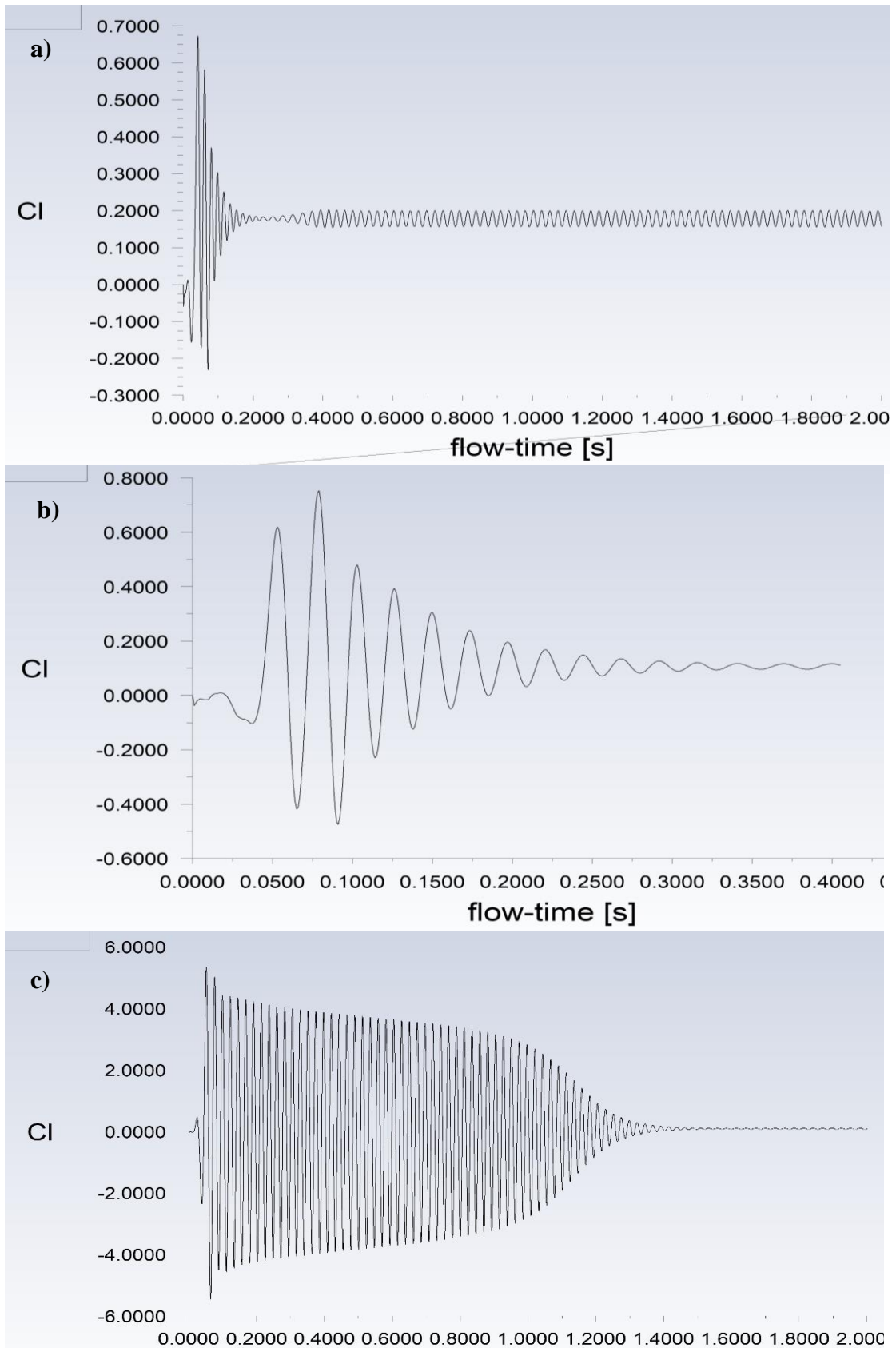


Figure 17: Coefficient of lift of square prism with larger circular cylinder upstream for velocity of a) 10, b) 7.8, and c) 7.5 m/s

As we plot the Frequency VS velocity graph, a linear relationship is found for velocity range of 1 m/s to up to near 7.5 m/s. Here, the frequency ( $f_{s0}$ ) is the nonvibrating vortex-shedding frequency. This follows the Strouhal law and the average Strouhal number can be obtained from the graph as 0.2132 which agrees with the existing standard value. Shedding frequency is inversely proportional to characteristic length limiting the geometry of the harvester from being too small. From the CFD analysis, we can conclude that the proposed energy harvester has the potential for piezoelectric energy harvesting from wake-induced vortices. For further analysis system coupling or fluid structure interaction is necessary.

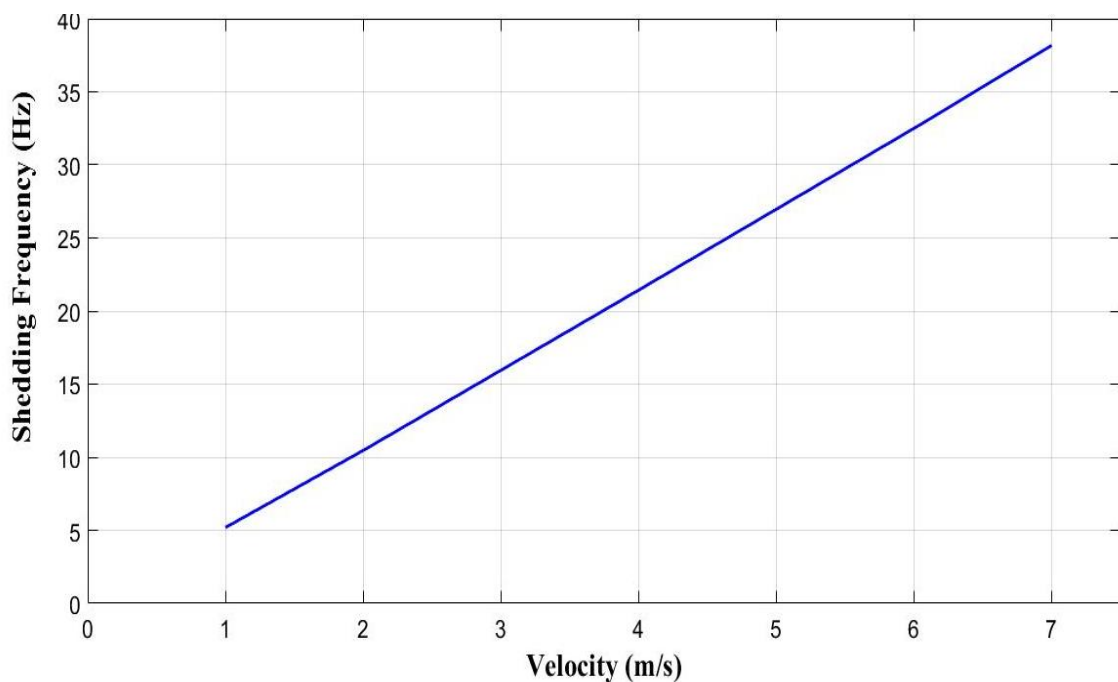


Figure 18: Non-vibrating vortex shedding frequency at different velocities

### 5.3 FSI Simulation: System Coupling

The fluid structure interaction simulation using the piezoelectric patch within the transient structure solver was run for 4m/s inlet velocity. The piezoelectric patch of thickness 1mm and 0.3mm were tested that produced sinusoidal voltage with peak of 1.2 V and 1.59 V respectively. Similarly experimental study was also carried out at wind tunnel of Pulchowk campus at 2.18 m/s velocity using piezoelectric sensor and Arduino programming. More simulations were run at inlet velocities of 1 m/s and 10 m/s. The peak voltage at 1, 2.18, 4 and 10 m/s are 0.17, 1.37, 1.59 and 0.2 respectively. The result agrees with CFD and vibration is decrease after shear layer reattachment.

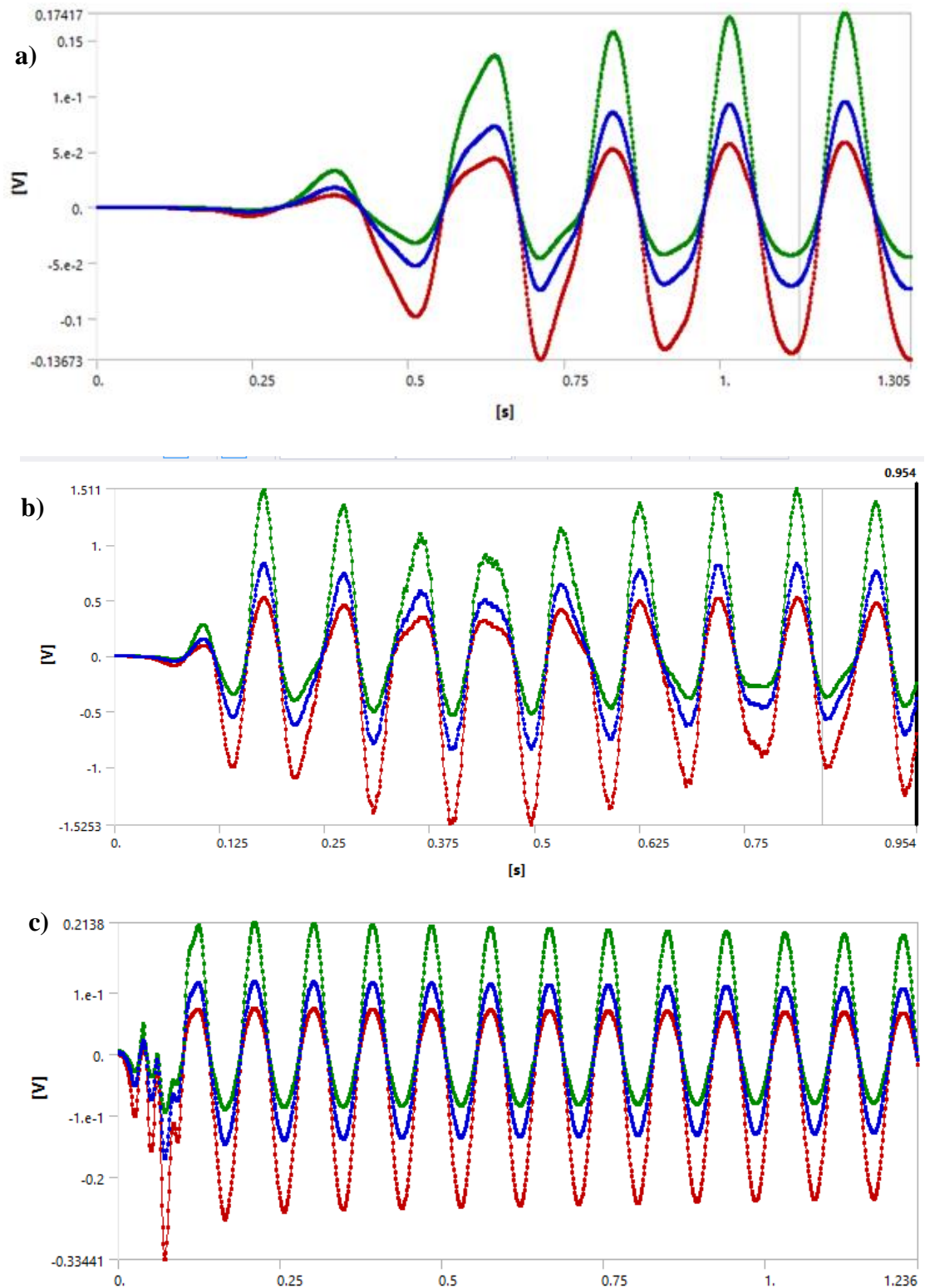


Figure 19: Values of maximum, average and minimum voltages generated for inlet velocities of a) 1 m/s, b) 4 m/s and c) 10 m/s



## 5.4 Experimental Study

The design setup was fabricated using steel. The prism of 16 mm width was made of mild steel and splitter plate length was maintained to obtained the same natural frequency of the numerical design. Circular piezoelectric sensor was connected to the Arduino microprocess from which voltage readings at all milliseconds were recorded in the personal computer. Experiment was carried out at this set up and simulation was also run designing the similar setup.



Figure 210: Fabrication process for experimental study

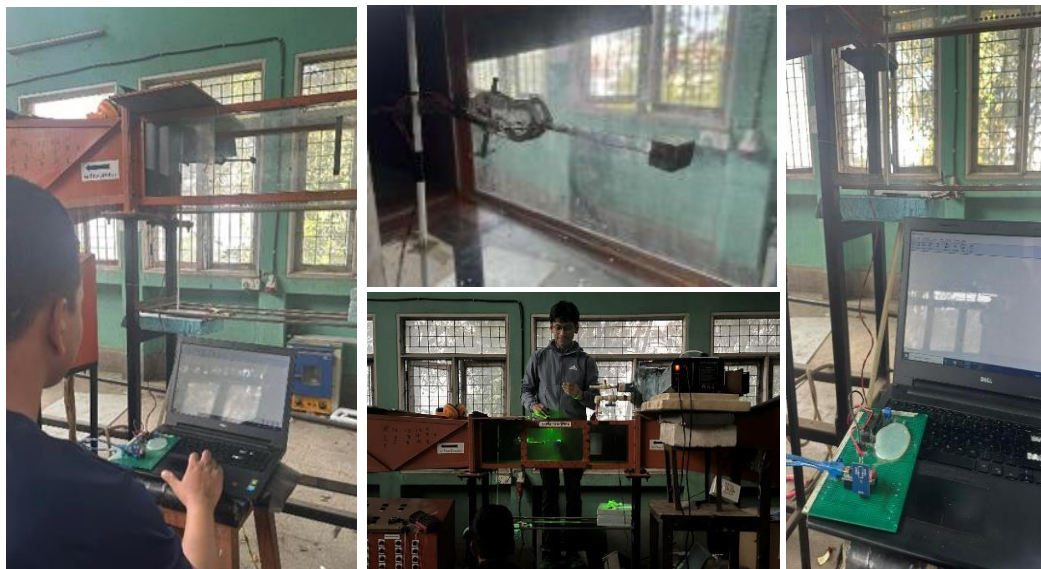


Figure 201: Experimental setup at wind tunnel in Pulchowk campus

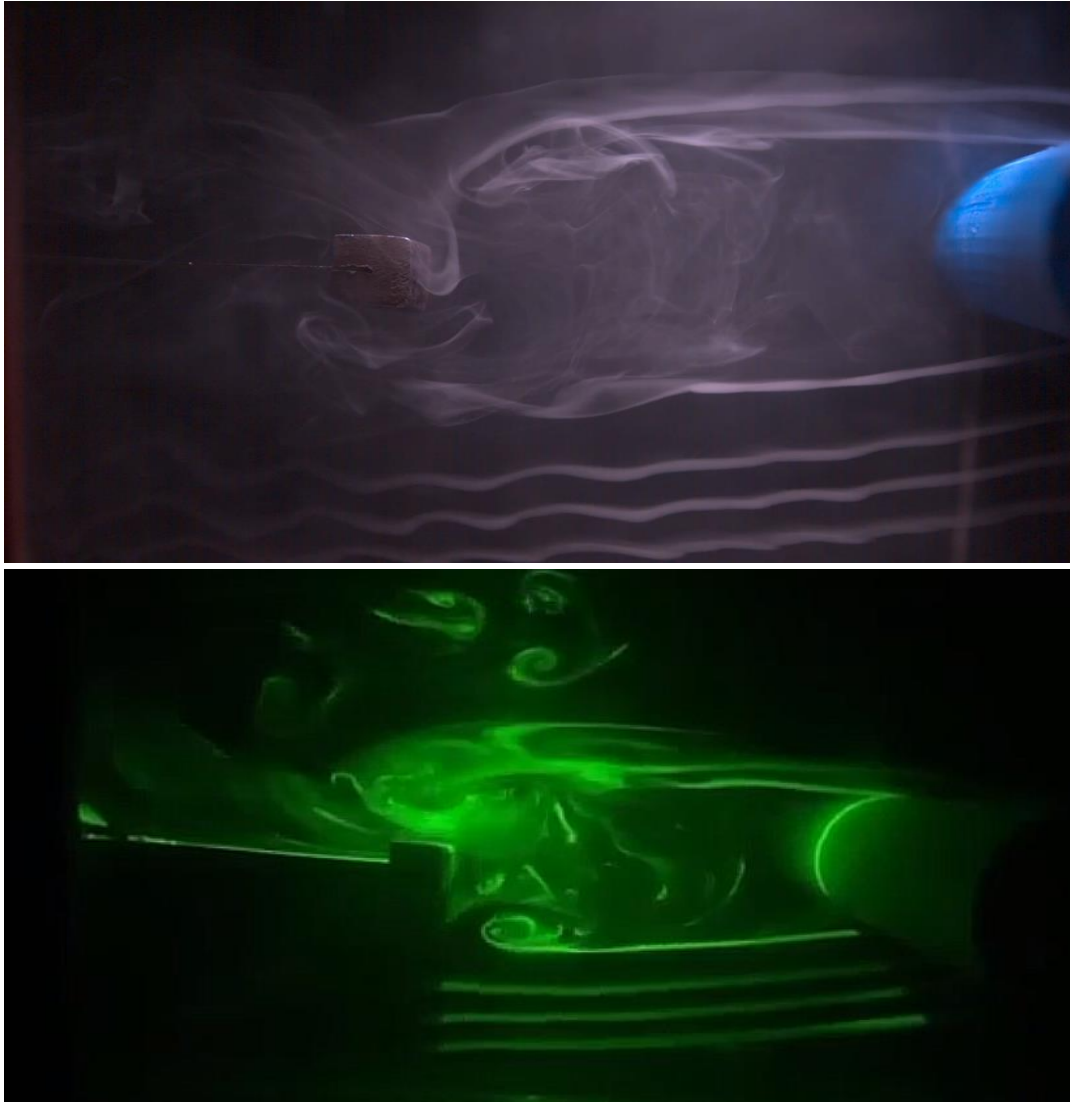


Figure 22: Flow Visualization at  $Re = 1354$  at wind tunnel in Pulchowk Campus

During the experiment only positive cycle of the voltage was plotted due to directional limitation of the Arduino microprocessor that can be reproduced on both sides if needed for the study. The sinusoidal AC-like Voltage was generated with frequency of 9.7 Hz that is around 14% less than the numerical and theoretical frequency of 11.3 Hz which is a fairly good result for these types of studies. However, the amplitude of the voltage obtained from the experiment was much lower than obtained from simulation. This can be attributed to various limitations in the experimental study such as quality of PZT sensor, contact between PZT patch and splitter plate, material property of the PZT patch, fabrication defects, irregularities, wind tunnel limitations, losses etc.

The energy harvester can be fabricated with significantly improved performance if advanced manufacturing approaches are taken. From the study, we can conclude that the proposed energy harvester has the potential for piezoelectric energy harvesting at the studied low velocity and small dimensional regimes and can be further enhanced with future studies.

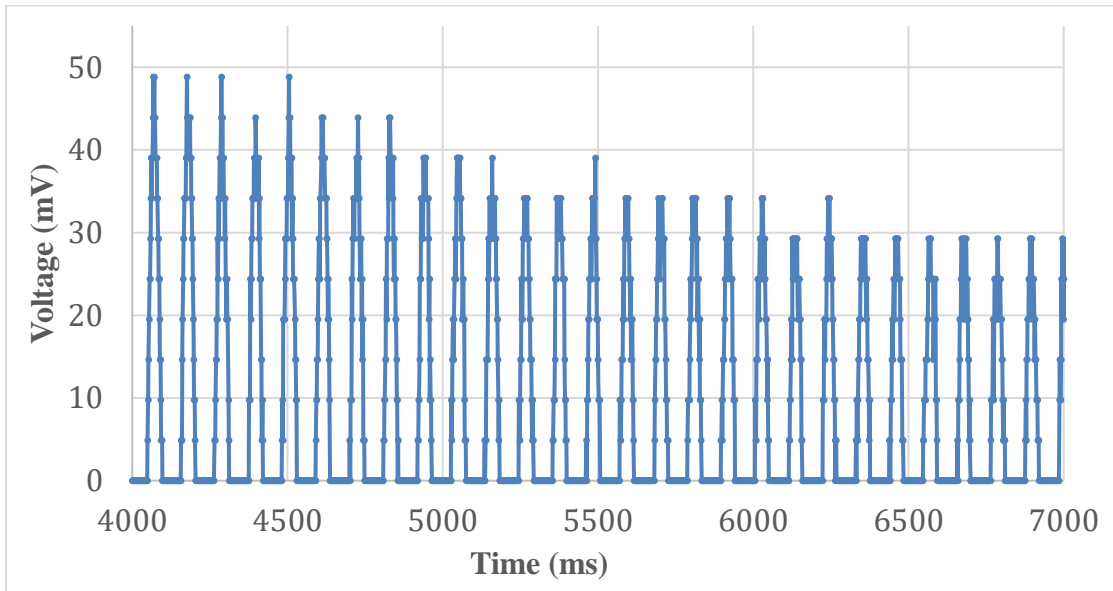


Figure 23: Experimental value of Positive Voltage readings of PZT sensor through arduino interface

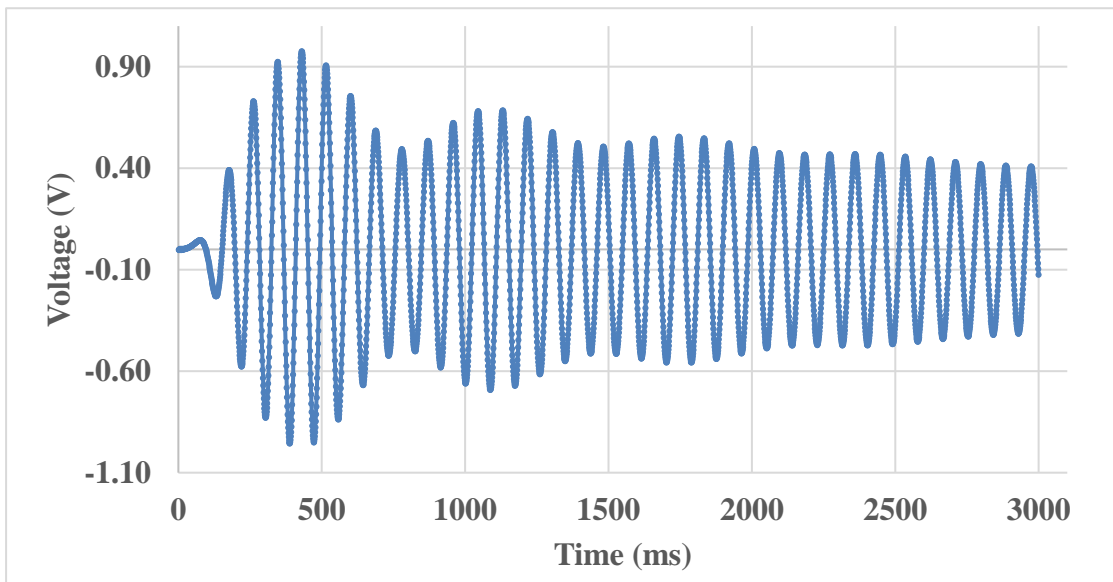


Figure 24: Average Voltage obtained from FSI Simulation

## CHAPTER 6: CONCLUSION AND FUTURE ENHANCEMENTS

### 6.1 Conclusion

As per the motive of the study, the designed energy harvester is found effective at the chosen regime of low flow velocity and small structural dimensional. Upto 7 m/s, using upstream larger cylinder helped to generate fluctuating wake that produces sinusoidal lift on secondary cylinder. Beyond that shear layer reattachment is seen. The results of the numerical study were found to be valid when compared to standard values of dimensionless parameters at this experimental regime. CFD analysis shows the energy harvester can perform well from 1 m/s to 7 m/s. The arrangement of cylinder at 3D, use of splitter plate, frequency synchronization at 2 m/s, all worked to enhance the performance of the energy harvester. FSI Simulation was done for inlet velocity of 4 m/s which generated sinusoidal emf with peak voltage of 1.2V and 1.59 V for piezoelectric plate of 1mm and 0.3mm thickness. The experimental setup was created with circular piezoelectric patch whose result showed voltage generation pattern similar to the simulation that was done mimicking the exact experimental setup. From the study, we can conclude that the proposed energy harvester has the potential for piezoelectric energy harvesting at the studied low velocity and small dimensional regimes. It can also serve as a reference for future studies and the performance of this piezoelectric energy harvester can be further enhanced with further explorations and research.

### 6.2 Future Enhancements

Since electric load can act as damper reducing vibration of transient structure, a three-way system coupling between fluid, solid and electric parameters can provide better numerical study as well as can enable us to quantify the value of energy that can be generated.

The experiment and simulation can be carried in a greater number of velocities and more setup variation using greater computational power and design iterations can be made along the study resulting in better configurations and design. Use of advanced manufacturing techniques as well as advanced materials and future optimizations may result in the harvester being practically feasible for energy generation applications.

## REFERENCES

1. Abdelkefi, A., Litak, G., & Wolszczak, P. (2022). Preface of the “Symposium on Nonlinear Energy Harvesting from Mechanical and Aeroelastic Vibrations.” 410001. <https://doi.org/10.1063/5.0082041>
2. Cao, D., Wang, J., Guo, X., Lai, S. K., & Shen, Y. (2022). Recent advancement of flow-induced piezoelectric vibration energy harvesting techniques: Principles, structures, and nonlinear designs. *Applied Mathematics and Mechanics*, 43(7), 959–978. <https://doi.org/10.1007/s10483-022-2867-7>  
<https://doi.org/10.1016/j.jfluidstructs.2022.103751>
3. Gautam, A., & Luintel, M. C. (n.d.). Study of a Flow-Induced-Vibration Energy Harvester: A Case of Two-degree of Freedom Galloping Based Scheme.
4. Latif, U., Uddin, E., Abdullah, C., Ali, Z., Sajid, M., Akhtar, K., & Shah, S. R. (2020). Experimental investigation of energy harvesting behind a bluff body. *Journal of Renewable and Sustainable Energy*, 12(3), 033301. <https://doi.org/10.1063/1.5144347>
5. Lee, Y. J., Qi, Y., Zhou, G., & Lua, K. B. (2019). Vortex-induced vibration wind energy harvesting by piezoelectric MEMS device in formation. *Scientific Reports*, 9(1), 20404. <https://doi.org/10.1038/s41598-019-56786-0>
6. Li, D., Wu, Y., Da Ronch, A., & Xiang, J. (2016). Energy harvesting by means of flow-induced vibrations on aerospace vehicles. *Progress in Aerospace Sciences*, 86, 28–62. <https://doi.org/10.1016/j.paerosci.2016.08.001>
7. Li, Z., Liu, K., Zhao, C., Zhou, B., Yang, Y., & Zhang, G. (2022). A Dual-Beam Coupled System for Hybrid Galloping and Vortex-Induced Vibration Energy Harvesting. *Symmetry*, 14(12), 2601. <https://doi.org/10.3390/sym14122601>
8. Liu, C., & Li, Z. (2011). On the validity of the Navier-Stokes equations for nanoscale liquid flows: The role of channel size. *AIP Advances*, 1(3), 032108. <https://doi.org/10.1063/1.3621858>
9. Parameshwaran, R., Dhulipalla, S. J., & Yendluri, D. R. (2016). Fluid-structure Interactions and Flow Induced Vibrations: A Review. *Procedia Engineering*, 144, 1286–1293. <https://doi.org/10.1016/j.proeng.2016.05.124>
10. Perera, S. M. H. D., Putrus, G., Conlon, M., Narayana, M., & Sunderland, K. (2022). Wind Energy Harvesting and Conversion Systems: A Technical Review. *Energies*, 15(24), 9299. <https://doi.org/10.3390/en15249299>

11. Rostami, A. B., & Armandei, M. (2017). Renewable energy harvesting by vortex-induced motions: Review and benchmarking of technologies. *Renewable and Sustainable Energy Reviews*, *70*, 193–214. <https://doi.org/10.1016/j.rser.2016.11.202>
12. Shang, L., Hoareau, C., & Zilian, A. (2022). Modeling and simulation of thin-walled piezoelectric energy harvesters immersed in flow using monolithic fluid–structure interaction. *Finite Elements in Analysis and Design*, *206*, 103761. <https://doi.org/10.1016/j.finel.2022.103761>
13. Sun, W., Zhao, D., Tan, T., Yan, Z., Guo, P., & Luo, X. (2019). Low velocity water flow energy harvesting using vortex induced vibration and galloping. *Applied Energy*, *251*, 113392. <https://doi.org/10.1016/j.apenergy.2019.113392>
14. Thakur, S. (2019). Aeroelastic Energy Harvesting: A Case for Galloping.
15. Villa, F., Sánchez, C., Vallejo, M., Botero-Valencia, J. S., & Delgado-Trejos, E. (2021). Dataset of Flow-Induced Vibrations on a Pipe Conveying Cold Water. *Data*, *6*(9), 100. <https://doi.org/10.3390/data6090100>
16. Wang, J., Geng, L., Ding, L., Zhu, H., & Yurchenko, D. (2020). The state-of-the-art review on energy harvesting from flow-induced vibrations. *Applied Energy*, *267*, 114902. <https://doi.org/10.1016/j.apenergy.2020.114902>
17. Wang, J., Li, G., Zhang, M., Zhao, G., Jin, Z., Xu, K., & Zhang, Z. (2018). Energy harvesting from flow-induced vibration: A lumped parameter model. *Energy Sources, Part A: Recovery, Utilization, and Environmental Effects*, *40*(24), 2903–2913. <https://doi.org/10.1080/15567036.2018.1513100>
18. Wang, J., Yurchenko, D., Hu, G., Zhao, L., Tang, L., & Yang, Y. (2021a). Perspectives in flow-induced vibration energy harvesting. *Applied Physics Letters*, *119*(10), 100502. <https://doi.org/10.1063/5.0063488>
19. Wang, J., Zhang, C., Zhang, M., Abdelkefi, A., Yu, H., Ge, X., & Liu, H. (2021). Enhancing energy harvesting from flow-induced vibrations of a circular cylinder using a downstream rectangular plate: An experimental study. *International Journal of Mechanical Sciences*, *211*, 106781. <https://doi.org/10.1016/j.ijmecsci.2021.106781>
20. Wu, Y., Li, D., & Xiang, J. (2015, January 5). Performance Analysis and Parametric Design of an Airfoil-Based Piezoaeroelastic Energy Harvester. *56th AIAA/ASCE/AHS/ASC Structures, Structural Dynamics, and Materials Conference*. 56th AIAA/ASCE/AHS/ASC Structures, Structural Dynamics, and

- Materials Conference, Kissimmee, Florida. <https://doi.org/10.2514/6.2015-0445>
21. Wu, Y., Li, D., Xiang, J., & Da Ronch, A. (2017). Piezoaeroelastic energy harvesting based on an airfoil with double plunge degrees of freedom: Modeling and numerical analysis. *Journal of Fluids and Structures*, 74, 111–129. <https://doi.org/10.1016/j.jfluidstructs.2017.06.009>
  22. Zhang, L. B., Abdelkefi, A., Dai, H. L., Naseer, R., & Wang, L. (2017). Design and experimental analysis of broadband energy harvesting from vortex-induced vibrations. *Journal of Sound and Vibration*, 408, 210–219. <https://doi.org/10.1016/j.jsv.2017.07.029>
  23. Zhu, H., Tang, T., Yang, H., Wang, J., Song, J., & Peng, G. (2021). The State-of-the-Art Brief Review on Piezoelectric Energy Harvesting from Flow-Induced Vibration. *Shock and Vibration*, 2021, 1–19. <https://doi.org/10.1155/2021/8861821>
  24. Zhu, H., Zhao, Y., & Zhou, T. (2018). CFD analysis of energy harvesting from flow induced vibration of a circular cylinder with an attached free-to-rotate pentagram impeller. *Applied Energy*, 212, 304–321. <https://doi.org/10.1016/j.apenergy.2017.12.059>
  25. Ma, C., Wan, D., & Yuan, Z. (n.d.). *Three-Dimensional Numerical Simulation of Vortex-Induced Vibration of a Rigid Cylinder*.
  26. Turek, S., & Hron, J. (2006). Proposal for Numerical Benchmarking of Fluid-Structure Interaction between an Elastic Object and Laminar Incompressible Flow. In H.-J. Bungartz & M. Schäfer (Eds.), *Fluid-Structure Interaction* (Vol. 53, pp. 371–385). Springer Berlin Heidelberg. [https://doi.org/10.1007/3-540-34596-5\\_15](https://doi.org/10.1007/3-540-34596-5_15)
  27. Vicente Ludlam, D. (2017). *Optimal energy harvesting from vortex-induced and transverse galloping vibrations* [PhD Thesis, Universidad Politécnica de Madrid]. <https://doi.org/10.20868/UPM.thesis.45545>
  28. Maruai, N. M., Ali, M. S. M., Ismail, M. H., & Zaki, S. A. (2018). Flow-induced vibration of a square cylinder and downstream flat plate associated with micro-scale energy harvester. *Journal of Wind Engineering and Industrial Aerodynamics*, 175, 264–282. <https://doi.org/10.1016/j.jweia.2018.01.01>

# PLAGIARISM CHECK

## Wake induced vibration for energy harvesting

### ORIGINALITY REPORT

12%

SIMILARITY INDEX

### PRIMARY SOURCES

- 1 [www.researchgate.net](http://www.researchgate.net)  
Internet 156 words — 1%
- 2 Junlei Wang, Chengyun Zhang, Mingjie Zhang, Abdessattar Abdelkefi, Haiyan Yu, Xiaomeng Ge, Huadong Liu. "Enhancing energy harvesting from flow-induced vibrations of a circular cylinder using a downstream rectangular plate: an experimental study", International Journal of Mechanical Sciences, 2021  
Crossref 140 words — 1%
- 3 Md.Mahbub Alam, M Moriya, K Takai, H Sakamoto. "Fluctuating fluid forces acting on two circular cylinders in a tandem arrangement at a subcritical Reynolds number", Journal of Wind Engineering and Industrial Aerodynamics, 2003  
Crossref 94 words — 1%
- 4 [m.moam.info](http://m.moam.info)  
Internet 53 words — < 1%
- 5 [e-jamet.org](http://e-jamet.org)  
Internet 34 words — < 1%
- 6 Jjian Lian, Zhichuan Wu, Shuai Yao, Xiang Yan, Xiaoqun Wang, Zhaolin Jia, Yan Long, Nan Shao, Defeng Yang, Xinyi Li. "Experimental Investigation of Flow-Induced Motion and Energy Conversion for Two Rigidly